การหาตำแหน่งอ้างอิงสำคัญจากภาพรังสีวัดศีรษะแบบอัตโนมัติ

นางสาวเฉลิมขวัญ ศิริพันธุ์

วิทยานิพนธ์นี้เป็นส่วนหนึ่งของการศึกษาตามหลักสูตรปริญญาวิทยาศาสตรมหาบัณฑิต
สาขาวิชาวิศวกรรมชีวเวช (สหสาขาวิชา)
คณะวิศวกรรมศาสตร์ จุฬาลงกรณ์มหาวิทยาลัย
ปีการศึกษา 2555

ลิขสิทธิ์ของจุฬาลงกรณ์มหาวิทยาลัย

บทคัดย่อและแฟ้มข้อมูลฉบับเต็มของวิทยานิพนธ์ตั้งแต่ปีการศึกษา 2554 ที่ให้บริการในคลังปัญญาจุฬาฯ (CUIR)
เป็นแฟ้มข้อมูลของนิสิตเจ้าของวิทยานิพนธ์ที่ส่งผ่านทางบัณฑิตวิทยาลัย

The abstract and full text of theses from the academic year 2011 in Chulalongkorn University Intellectual Repository(CUIR)
are the thesis authors' files submitted through the Graduate School.

AUTOMATIC CEPHALOMETRIC LANDMARKS DETECTION

Miss Chalermkwan Siripanth

A Thesis Submitted in Partial Fulfillment of the Requirements

for the Degree of Master of Science Program in Biomedical Engineering

(Interdisciplinary Program)

Faculty of Engineering

Chulalongkorn University

Academic Year 2012

Thesis Title	AUTOMATIC CEPHALOMETRIC LANDMARKS DETECTION
By	Miss Chalermkwan Siripanth
Field of Study	Biomedical Engineering
Thesis Advisor	Associate Professor Nongluk Covavisarach
Thesis Co-advisor	Assistant Professor Paiboon Techalertpaisarn, DDS., Ph.D.

Accepted by the Faculty of Engineering, Chulalongkorn University in Partial Fulfillment of the Requirements for the Master's Degree

……. Dean of the Faculty of Engineering
(Associate Professor Boonsom Lerdhirunwong, Dr.Ing.)

THESIS COMMITTEE

…….. Chairman
(Associate Professor Mana Sriyudthsak, Ph.D.)

……. Thesis Advisor
(Associate Professor Nongluk Covavisarach)

…….. Thesis Co-advisor
(Assistant Professor Paiboon Techalertpaisarn, DDS., Ph.D.)

…….. External Examiner
(Assistant Professor Bundit Thipakorn, Ph.D.)

เฉลิมขวัญ ศิริพันธุ์ : การหาตำแหน่งอ้างอิงสำคัญจากภาพรังสีวัดศีรษะแบบอัตโนมัติ (AUTOMATIC CEPHALOMETRIC LANDMARKS DETECTION) อ. ที่ปรึกษาวิทยานิพนธ์หลัก : รศ. นงลักษณ์ โควาวิสารัช , อ. ที่ปรึกษาวิทยานิพนธ์ร่วม : ผศ. ดร. ไพบูลย์ เตชะเลิศไพศาล, 82 หน้า.

ตำแหน่งอ้างอิงสำคัญจากภาพรังสีวัดศีรษะเป็นสิ่งพื้นฐานและสำคัญสำหรับการวิเคราะห์กะโหลกศีรษะเพื่อใช้ในการวิเคราะห์ วินิจฉัยโครงสร้างใบหน้าของมนุษย์ วิธีการดั้งเดิมในการกำหนดจุดภาพรังสีวัดศีรษะดังกล่าวจะให้ทันตแพทย์ผู้เชี่ยวชาญเป็นผู้วาดโครงร่างใบหน้าขึ้นมาด้วยมือ ด้วยการลอกลาย จากนั้นจะพิจารณาจาก ความรู้ทางกายวิภาคศาสตร์ร่วมด้วยเพื่อให้ได้ตำแหน่งอ้างอิงสำคัญจากภาพรังสีแต่ละจุด จะเห็นได้ว่า ขั้นตอนดังกล่าวต้องใช้เวลา และเป็นงานที่ขึ้นกับแต่ละตัวบุคคล เพื่อหลีกเลี่ยงข้อเสียดังกล่าว จึงมีผู้คิดค้นระบบคอมพิวเตอร์เพื่อใช้ในการหาตำแหน่งอ้างอิงสำคัญจากภาพรังสีทั้งอัตโนมัติ และกึ่งอัตโนมัติ

การทดลองของเราใช้การวิเคราะห์โปรครัสต์ (Procrustes Analysis) สร้างโมเดลขึ้นมาสำหรับโครงสร้างใบหน้า โดยแบ่งเป็นสองส่วน คือ ส่วนบนของใบหน้ากับส่วนล่างของใบหน้า เมื่อมีภาพใบหน้าภาพใหม่เข้ามา ระบบจะเริ่มจากการหาจุดอ้างอิงเบื้องต้นเพื่อใช้ในการวางโมเดล หลังจากวางโมเดลแล้ว พื้นที่ที่สนใจสำหรับแต่ละจุดกำหนดภาพรังสีจะถูกกำหนดโดยพิจารณาจากตำแหน่งจากโมเดล และความรู้ทางกายวิภาคร่วมด้วย

การทดลองของเราประเมินผลด้วย อัลกอริทึ่ม Leave-one-out ผลที่ได้พบว่า การเจอจุดกำหนดภาพรังสีภายในพื้นที่ที่สนใจสำหรับส่วนบนของใบหน้าคิดเป็น 85.84% และส่วนล่างคิดเป็น 83.33% สำหรับการคำนวณระยะความผิดพลาด จะมีการประเมินความแม่นยำของผู้เชี่ยวชาญโดยให้ผู้เชี่ยวชาญทำการจุดจุดกำหนดภาพรังสีจุดเดิมจำนวน 2 ครั้งที่ทิ้งช่วงเวลาห่างกันพอประมาณ จากการทดลองพบว่า วิธีการที่นำเสนอมีความแม่นยำในการค้นหาจุดกำหนดภาพรังสีได้ใกล้เคียงกับแพทย์ผู้เชี่ยวชาญ ยิ่งไปกว่านั้น จุดกำหนดภาพรังสีบางจุดยังได้ผลลัพธ์ที่ดีกว่าการกำหนดโดยแพทย์

จากจำนวนจุดกำหนดรังสีทั้งหมด 13 จุด พบว่า มี 8 จุดที่มีค่าความคลาดเคลื่อนน้อยกว่า 3 มม. และมีเพียง 2 จุด ที่มีค่าความคลาดเคลื่อนมากกว่า 5 มม.

สาขาวิชา วิศวกรรมชีวเวช ลายมือชื่อนิสิต .....

ปีการศึกษา 2555 ลายมือชื่อ อ.ที่ปรึกษาวิทยานิพนธ์หลัก .....

ลายมือชื่อ อ.ที่ปรึกษาวิทยานิพนธ์ร่วม .....

5287129321 : MAJOR BIOMEDICAL ENGINEERING

KEYWORDS : CEPHALOMETRIC LANDMARK/ AUTOMATIC DETECTION

CHALERMKWAN SIRIPANTH : AUTOMATIC CEPHALOMETRIC LANDMARKS DETECTION. ADVISOR : ASSOC. NONGLUK COVAVISARUCH, CO-ADVISOR : ASST.PROF. PAIBOON TECHALERTPAISARN, DDS., Ph.D.

82 pp.

Cephalometric landmarks are required for Cephalometric analysis that is used in orthodontic analysis and human facial structure diagnosis. Thus, in order to reduce time and needs of expert orthodontists, many attempts have been proposed to use computers instead of manual procedure to acquire those landmarks. Our proposed method is to create two non-deformable general models by Procrustes analysis, one for the upper part and the other, the lower, of a human facial structure. By placing and aligning the general models on a test image, considering some anatomical conditions, regions of interest (ROI's) of the target landmarks are automatically identified.

Our algorithm is evaluated by leave-one-out method, it is found that the average success rates of finding the landmarks within the +/- 2 SD ROI's are 85.84% and 83.33% for the upper and the lower models respectively. For error calculation, an expert orthodontist has been asked to locate landmark twice for some images in order to evaluate the expert accuracy. We found that our methodology gave the accuracy of some landmarks as similar as the expert. Moreover, some detection gave better results than an expert.

From 13 landmarks, 8 landmarks were detected within 3 mm. error, while only 2 landmarks were detected with more than 5 mm. error.

Field of Study : Biomedical Engineering Student's Signature .....

Academic Year : 2012 Advisor's Signature .....

Co-advisor's Signature .....

Acknowledgements

I have been supported in so many ways throughout my research and everything leading up to this point. Foremost, I wish to express my faithful to my advisor, Associate Professor Nongluk Covavisaruch and my co-advisor, Assistant Professor Dr. Paiboon Techalertpaisarn for their assistance and encouragement in conducting this research.

I also gratefully acknowledge the members of my thesis committee, Associate Professor Dr. Mana Sriyudthsak and Assistant Professor Dr. Bundit Thipakorn for their discussion and guidance.

In addition, many thanks go as well to the whole Computer Graphic and Computer Intelligent (CGCI) group in the Department of Computer Engineering and the whole Biomedical Engineering (BME) group, Faculty of Engineering, Chulalongkorn University, especially to Associate Professor Nongluk Covavisaruch, for fruitful discussions and ideas. Thanks to all of them and the working environment is exemplary.

Furthermore, I am grateful to the ChulalongKorn University Graduate Scholarship for my two first year financial support and also inter-conference financial support.

Moreover, thanks to Toshiba International Foundation (TIFO) who granted me a to be as a temporary researcher in Image Processing Laboratory, Research and Development center, Toshiba, Japan for 3 months. The comprehensive training from Toshiba improves not only my programming skill, but also my working style.

Last but not least, special thanks to my family especially my father who support and encourage me throughout this study and my everyday life. I am very thankful to my friends for their friendship and their help during my graduate study.

Contents

Page

Abstract (Thai)..... iv

Abstract (English)..... v

Acknowledgements..... vi

Contents..... vii

List of Tables..... x

List of Figures..... xi

Chapter

I Introduction..... 1

1.1 Background and motivation..... 1

1.2 Objectives..... 2

1.3 Scope..... 2

1.4 Contribution..... 3

1.5 Thesis Organization..... 3

II Literature Reviews..... 4

2.1 Dental Background..... 4

2.1.1 Cephalogram acquisition..... 4

2.1.2 Cephalometric landmarks..... 5

2.1.3 Cephalometric analysis..... 7

2.2 Computational Background..... 8

2.2.1 Procrustes analysis..... 8

2.2.2 Leave-one-out method..... 9

2.3 Image processing background..... 9

2.3.1 Digital Image Processing..... 9

2.3.2 Gaussian smoothing..... 10

2.3.3 Histogram specification..... 11

Chapter Page

2.3.4 Edge detection 13
2.3.5 Morphological image processing 14
2.4 Literature reviews 15
III Methodology 19
3.1 Overview 19
3.2 Select and group landmarks 20
3.3 Create models by Procrustes analysis 22
3.4 Calculate SD of general model 22
3.5 Pre-processing of recognition stage 24
3.6 Detect 3 reference landmarks 25
3.7 Place model using 3 reference landmarks 30
3.8 Specify ROI for each landmark 32
3.9 Locate each landmark 33
3.9.1 Porion. 33
3.9.2 Sella. 34
3.9.3 Orbitale. 34
3.9.4 ANS 35
3.9.5 Subspinale 35
3.9.6 Incisor superius and Incisor inferius 36
3.9.7 Supramentale and Pogonion. 37
3.9.8 Gonion 37
IV Experiments and Results 39
4.1 Materials 39
4.2 Computer specification and tools 40
4.3 Evaluation 40
4.3.1 Evaluate an expert (Intra-observer error) 40
4.3.2 Evaluate the general models 42
4.3.3 Comparison our error with Dahlberg's formula 43
4.3.4 Our results error calculated by Dahlberg's formula 44

Chapter Page

V Discussions and Conclusions 47
References 49
Appendices 53
Appendix A 54
Appendix B 68
Biography 82

List of Tables

Table		Page
2.1	40 primary cephalometric landmarks with anatomical name	6
3.1	Cephalometric landmarks in the first orthodontic analysis	21
4.1	Intra-observer error calculated by Dahlberg's formula.....	41
4.2	Success rate of finding cephalometric landmark in ROI (+/-2SD).....	42
4.3	Our results error calculated by Dahlberg's formula.....	43
4.4	Minimum, maximum and mean distance error of our results.....	45

List of Figures

Figure		Page
1.1	Points used in lateral cephalometric analysis	1
2.1	Distance for cephalogram acquisition	4
2.2	Average structure line when left and right side of organ are not completely overlaid	5
2.3	40 primary cephalometric landmarks on a draft of facial structure	5
2.4	An example of cephalometric analysis	7
2.5	An example of applying Procrustes analysis with point set of hand	9
2.6	Digital image processing	10
2.7	The relationship between cumulative histogram of input image and target image	12
2.8	Flow chart of histogram specification	12
2.9	Prewitt operators	13
2.10	Roberts operators	13
2.11	Sobel operators	13
3.1	Methodology flowchart	19
3.2	Procrustes analysis mean shape	22
3.3	Shape alignment for ROI specification	23
3.4	The area of image background used for calculating SD of Gaussian distribution	24
3.5	Result of pre-processing	25
3.6	Histogram specification results	26
3.7	Otsu thresholding	26
3.8	Result of line scanning	27
3.9	Ear rod detection	28
3.10	Nasion detection	29
3.11	Upper model alignment	30
3.12	Lower model alignment	31
3.13	ROI of each landmark	32

Figure Page

3.14 Porion detection 33
3.15 Sella detection 34
3.16 Orbitale detection 35
3.17 ANS detection 35
3.18 Subspinale detection 36
3.19 Incisor superior and inferius detection 36
3.20 Supramentale and Pogonion detection 37
3.21 Gonion detection 38
4.1 A cephalometric radiograph used in the thesis 39
4.2 Direction of errors 44
4.3 Incisor superior detection 46
4.4 Go detection 46
5.1 Non-symmetric organ causes two lines of mandibular plane..... 47

CHAPTER I

Introduction

1.1 Background and motivation

Orthodontics is a specialty of dentistry which is concerned about the study and treatment for abnormalities of head structure. And, the basic of diagnosis and treatment is an analysis of Cephalometric radiograph, called Cephalometric analysis. Thus, this analysis is a fundamental step in orthodontic field.

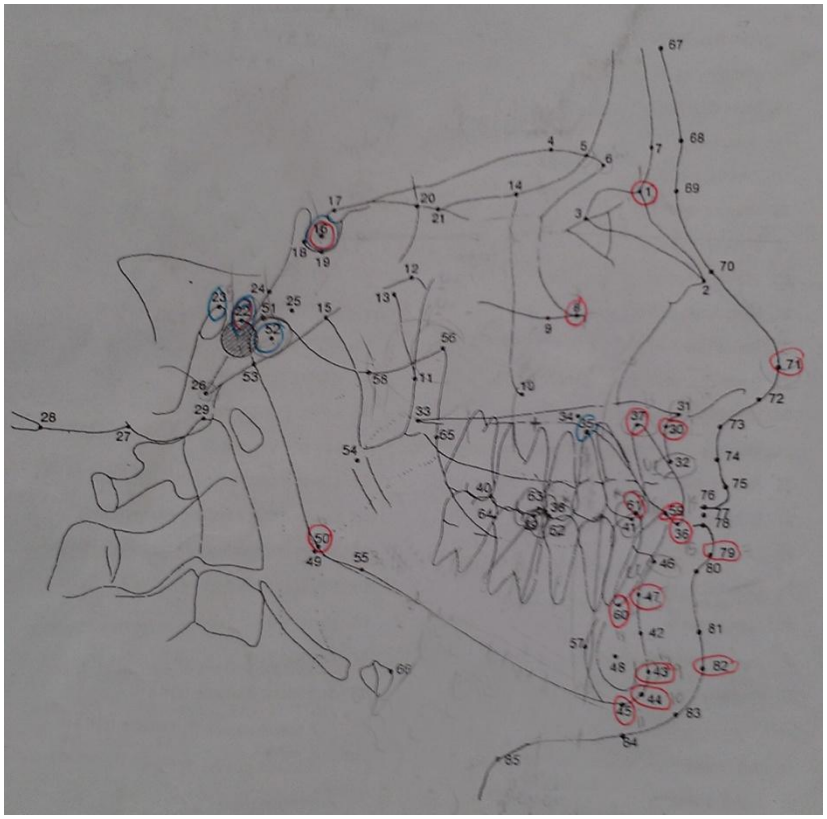

Figure 1.1 Points used in lateral cephalometric analysis [1]

The analysis is determined by identifying landmarks called Cephalometric landmarks which are located on both bone structure and soft tissue. There are about 200 landmarks covered on a lateral view of a human head structure. Some important landmarks are shown in Figure 1.1. To identify the landmarks, primitive method was done by human by overlaying a stencil paper on an X-ray image, then

tracing along the line of human head structure. Finally, the landmarks were identified by their anatomical definitions on the stencil paper of traced head structure. These processes are tedious. It's obviously seen that the important problem is time consumption. Moreover, the result depends on an orthodontist's experience. There's also a human error.

There are many attempts trying to solve the problems above using computer to detect the Cephalometric landmarks both fully-automatic and semi-automatic detection system. One of these attempts can be grouped as model-based approaches of which the main process is creating a model of a human head structure. According to the fact the composing a model with a large number of landmarks takes a lot of time. Since the more landmarks are used, the more robust the model is, time consumption has to be trading off the model's robustness.

Although most researches, which try to create a general model, implemented the system with a large number of landmarks, which are both pseudo and real Cephalometric landmarks, we tried to create the model with less landmarks in order to reduce an orthodontist's workload. Moreover, we created two models instead of one model as most researchers do. After placing a model, each landmark was identified individually using anatomical knowledge combined with gray scale image processing.

1.2 Objectives

1.2.1 Find methodology to detect Cephalometric landmarks automatically

1.2.2 Create tool for automatically finding Cephalometric landmarks

1.3 Scope

1.3.1 Not less than 30 Cephalometric images

1.3.2 Not less than 10 Cephalometric landmarks with less than +/- 5 mm average error compared with an expert

1.4 Contribution

Our aim is to help an orthodontist identify some of Cephalometric landmarks automatically. Moreover, since Cephalometric landmarks lead to Cephalometric analysis, the landmarks in this research will be used to calculate some value in the analysis.

1.5 Thesis Organization

This thesis is combined with 5 chapters. Next chapter of this thesis covers the dental knowledge and computational techniques used throughout this study. Besides, we explore the literatures related to this work. In chapter III, we demonstrate our methodology to our cephalogram detecting each landmark. Later on, Chapter IV shows the results of our experiments. Finally, we discuss and compare all results in chapter V.

CHAPTER II

Literature Reviews

In this chapter, we describe the fundamental knowledge consist of dental background, computational background and image processing background. Next, we review the literatures related to the Cephalometric landmark detection system.

2.1 Dental Background

2.1.1 Cephalogram acquisition [1]

Cephalogram is an X-ray image of patient's lateral head. The distance from x-ray source to mid-sagittal plane of patient is 60 inches and 15 inches from the mid-sagittal plane to film plane (see Figure 2.1). Moreover, obtained image may not be completely overlaid from left and right side of organ. The orthodontists have to approximate the average structure line before locate the landmarks (see Figure 2.2).

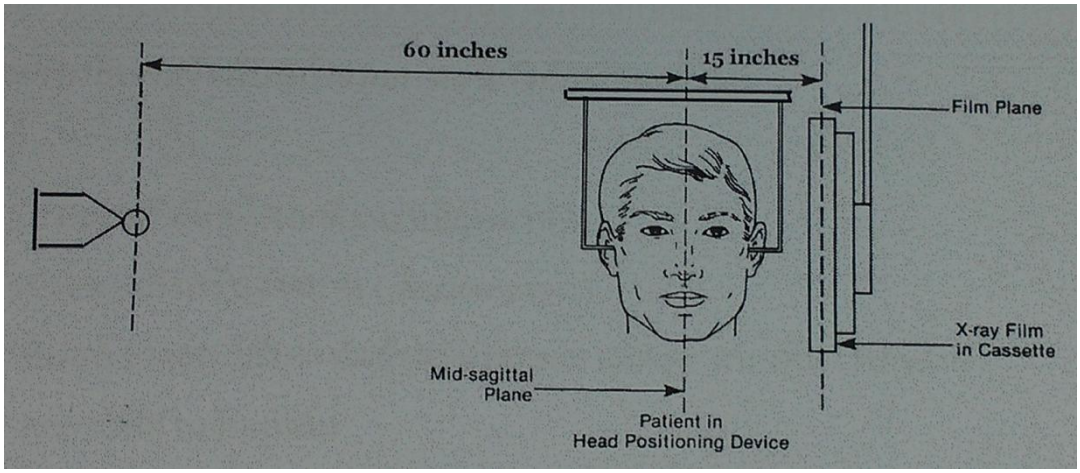

Figure 2.1 Distance for cephalogram acquisition [1]

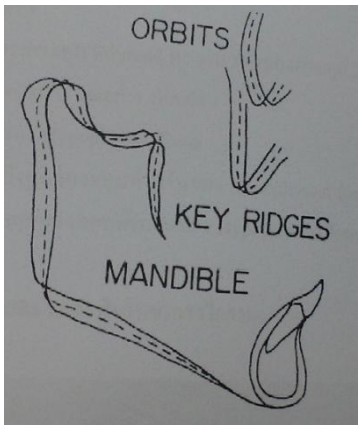

Figure 2.2 Average structure line when left and right side of organ are not completely overlaid [1]

2.1.2 Cephalometric landmarks

Cephalometric landmarks are the basis of cephalometric analysis. There is more than one definition for each landmark depends on each clinical use or reference. According to our expert orthodontist from department of orthodontics, faculty of dentistry, Chulalongkorn university, fourty cephalometric landmarks are used for representing a human's rough facial structure (see Figure 2.3). Each landmark has its anatomical name and definition as show in Table 2.1

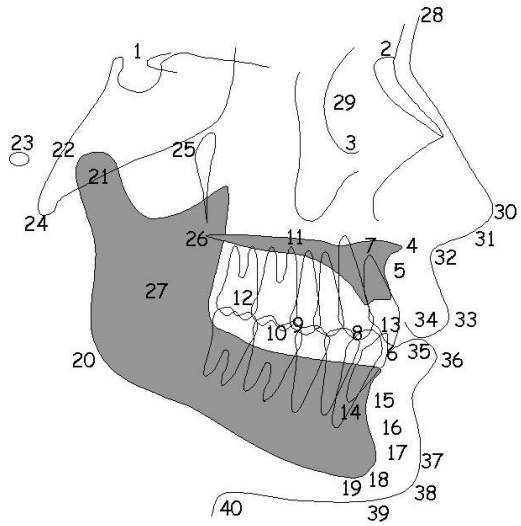

Figure 2.3 40 primary cephalometric landmarks on a draft of facial structure

Table 2.1 40 primary cephalometric landmarks with anatomical name [2]

No.	Name	No.	Name
1	Sella (S)	20	Gonion (Go)
2	Nasion (Na)	21	Capitulare (C)
3	Orbitale (Or)	22	Condylion (Ear rod)
4	Anterior Nasal Spine (ANS)	23	Porion (Po)
5	Subspinale (A)	24	Basion (Ba)
6	Incisor superius (Is)	25	Pterygoid point (Pt)
7	Upper incisor apex (UIA)	26	Posterior nasal spine (PNS)
8	Intersection of upper and lower first premolar	27	Xi point
9	Intersection of upper and lower first molar	28	Soft tissue glabella (G')
10	Upper molar mesial cusp (UMT)	29	Commisure of eye
11	Intersection of perpendicular line of perpendicular line of 8-9 line and palate lower border	30	Pronasion (Prn)
12	Upper first molar distal surface	31	Columella (Cm)
13	Incisor inferius (Ii)	32	Subnasion (Sn)
14	Lower incisor apex (LIA)	33	Labrale superius (Ls)
15	Supramentale (B)	34	Stomion superior (Sts)
16	Protuberance menti (Pm) (Point between 15 and 17)	35	Stomion inferior (Sti)
17	Pogonion (Pg)	36	Labrale inferius (Li)
18	Gnathion (Gn)	37	Soft tissue Pogonion (Pg')
19	Menton (Me)		

Table 2.1 (Continued)

No.	Name	No.	Name
38	Intersection of 36-37 line and 39-40 line	40	Cervical point
39	Soft tissue Menton (Me')		

2.1.2 Cephalometric analysis

Cephalometric Analysis is the analysis for studying human's facial growth and diagnosis the abnormalities in order to plan for the treatment. In practice, different cephalometric landmarks can be used in cephalometric analysis depending mainly on two factors; the type of analysis and an individual orthodontist's preference. Based on our expert, Figure 2.4 is an analysis used in department of orthodontics, faculty of dentistry, Chulalongkorn university. There are 19 landmarks used in the cephalometric analysis calculation as landmark number 1, 2, 3, 5, 6, 7, 8, 9, 13, 14, 15, 17, 18, 19, 20 , 23, 30, 36 and 37 (numbers are referenced from table 2.1 and figure 2.3)

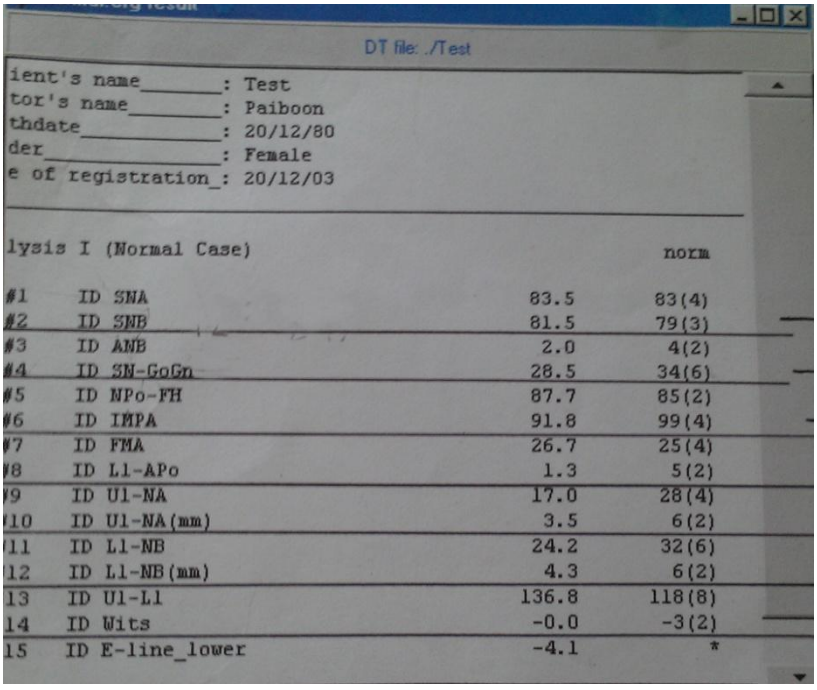
DT file: ./Test

ient's name_____: Test
tor's name_____: Paiboon
thdate_____: 20/12/80
der_____: Female
e of registration_: 20/12/03

lysis I (Normal Case) norm

#1	ID SNA	83.5	83(4)
#2	ID SNB	81.5	79(3)
#3	ID ANB	2.0	4(2)
#4	ID SN-GoGn	28.5	34(6)
#5	ID NPo-FH	87.7	85(2)
#6	ID IMPA	91.8	99(4)
#7	ID FMA	26.7	25(4)
#8	ID L1-APo	1.3	5(2)
#9	ID U1-NA	17.0	28(4)
#10	ID U1-NA(mm)	3.5	6(2)
#11	ID L1-NB	24.2	32(6)
#12	ID L1-NB(mm)	4.3	6(2)
#13	ID U1-L1	136.8	118(8)
#14	ID Wits	-0.0	-3(2)
#15	ID E-line_lower	-4.1	*

Figure 2.4 An example of cephalometric analysis

2.2 Computational Background

2.2.1 Procrustes analysis [3]

Procrustes analysis is well-know technique to represent shape correspondence which is an important aspect of imaging. It is a rigid shape analysis using isomorphic scaling, translation, and rotation to find the best fit between two or more landmarked shapes.

Algorithm for generalized orthogonal Procrustes analysis:

1. Select one shape to be the approximate mean shape (i.e. the first shape in the set)
2. Align the shape to the approximate mean shape.
   a. Calculate the centroid of each shape
   b. Align all shapes centroid to the origin
   c. Normalized each shapes *centroid size*
   d. Rotate each shape to align with the newest approximate mean
3. Calculate the new approximate mean from the aligned shapes
4. If the approximate mean from steps 2 and 3 are different, return to step 2, otherwise, the true mean shape of the set is found.

In addition, the centroid size is the most common measuring size of point set, calculated by the equation (2.1).

$$centroid\ size = \sqrt{\sum_{i=1}^{n}((x_i - \bar{x})^2 + (y_i - \bar{y})^2)} \quad (2.1)$$

where *n: number of landmarks*

$\bar{x}$ *:* average of x

$\bar{y}$ *:* average of y

$(\bar{x}, \bar{y})$ *: centroid of each shape*

Finally, after apply Procrustes analysis, the general shape of point set are obtained as shown in Figure 2.5

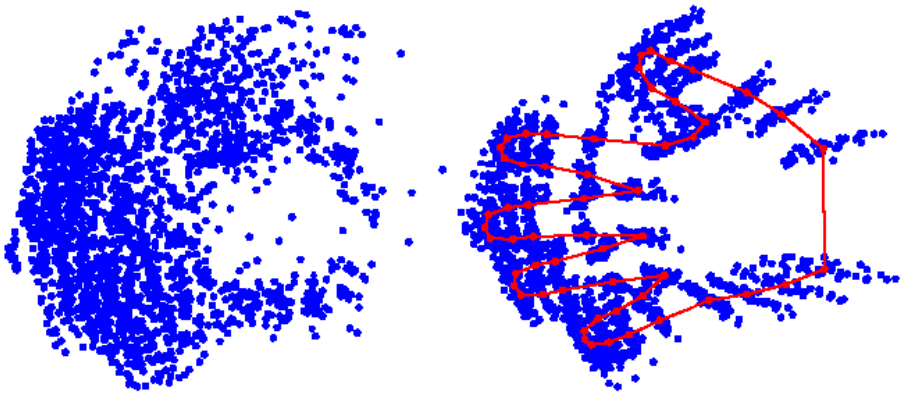

Figure 2.5 An example of applying Procrustes analysis with point set of hand

2.2.2 Leave-one-out method

Leave-one-out method is an unbiased and frequently used technique for model evaluation. It is an important statistical estimator of the performance of a learning algorithm [4]. A set of ground truth images (for example as N images) is split in N different combination into a training set of size N-1 and a test set of size 1. In addition, training a model is done on the N-1 images (training set) and then the remaining 1 image is tested. Performance is calculated as the average of N tests.

2.3 Image processing background

2.3.1 Digital Image Processing

Digital image processing is the use of computer algorithm to perform image processing on digital images [5]. The basic of digital image processing combines with 5 steps as follow (see Figure 2.6);

1. Image acquisition: The action of retrieving an image from some source, usually hardware such as a camera or a scanner.

2. Preprocessing: The procedure to correct image from various errors such as image distortion or noise.

3. Segmentation: The process of partitioning an image into a smaller part in order to make that region more meaningful, usually called “Region of interest (ROI)”

4. Representation and description: The process of extracting features in the region of interest

5. Recognition and interpretation: The final process to get the information from digital image

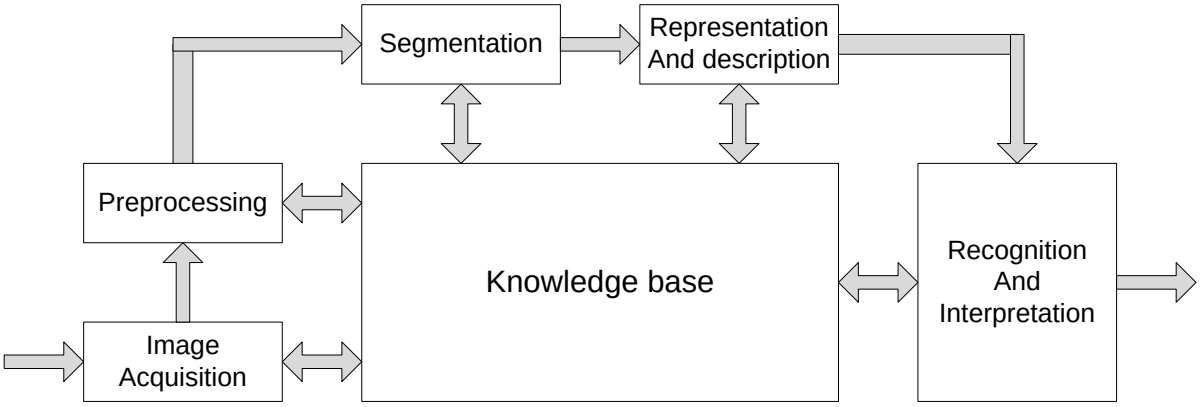

Figure 2.6 Digital image processing

2.3.2 Gaussian smoothing

Gaussian smoothing or Gaussian blur is a kind of preprocessing step as image enhancement in the frequency domain. It is a low-pass filter widely used to reduce a random noise. Mathematically, applying a Gaussian filter to an image is a convolution an image with a Gaussian function in equation 2.2.

$$g(x,y) = \frac{1}{2\pi\sigma^2} A e^{-\frac{(x^2+y^2)}{2\sigma^2}} \quad (2.2)$$

where (x, y) : a coordinate

σ: a standard deviation of Gaussian distribution

2.3.3 Histogram specification

Histogram specification is another algorithm of pre-processing to get the image whose histogram is the same shape as you desire. It uses nonlinear stretch operation, while histogram equalization use. Histogram specification is useful for image enhancement when you have the target shape of histogram and you want the same contrast and brightness of the two images. It also allows you to emphasize information in the exact brightness levels. Curve of histogram can be specified as any curve, for example, uniform, exponential, log, Gaussian, etc. [6]

There are 3 steps as follow [7];

1. Cumulate the equalized histogram (Px) of the input image (X) as y (equation 2.3)

$$y = f(x) = \int_0^x p_x(u)\,du \tag{2.3}$$

$p_x(u)$: Histogram of the input image

2. Cumulate the equalized histogram (Pz) of the desired image (Z) as y' (equation 2.4)

$$y' = g(z) = \int_0^z p_z(u)\,du \tag{2.4}$$

$p_z(u)$: Histogram of the desired image

3. Relate the two cumulative, equalized histograms by the processing in figure 2.7

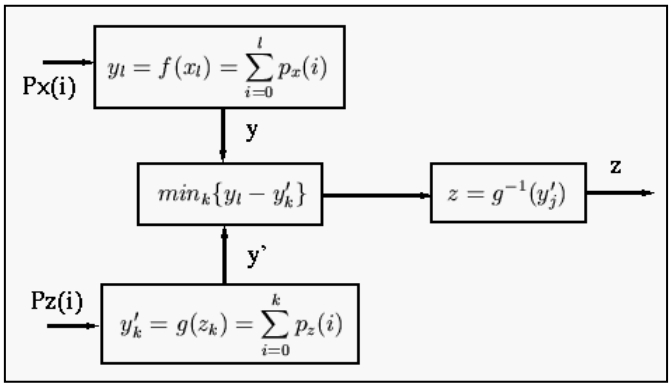

Figure 2.7 The relationship between cumulative histogram of input image and target image [6]

For conclusion (see Figure 2.8), process starts with tracking the gray value from the original image to probability in equalized histogram, then map that probability to the equalized histogram of desired image to specify the gray value.

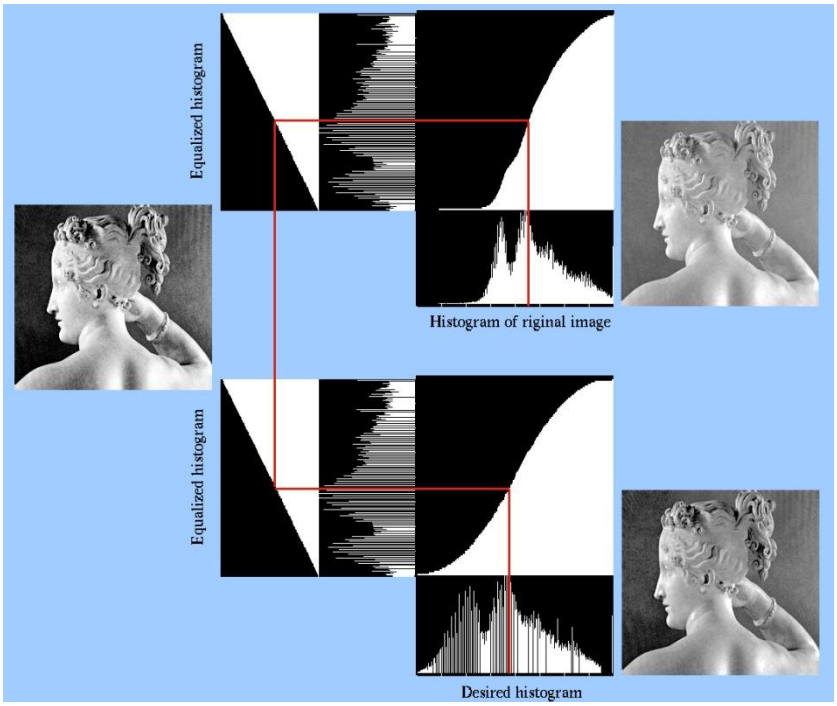

Figure 2.8 Flow chart of histogram specification [6]

2.3.4 Edge detection [8]

Edge detection is a process of image segmentation. It uses a set of the mathematic methods as a basis. There are many operators convoluted with image for detecting edges. Some basic operators are Prewitt operators (see Figure 2.8), Roberts operators (see Figure 2.9) and Sobel operators (see Figure 2.10). There are combinations of basic operators and other algorithms to detect edge such as Canny edge detector.

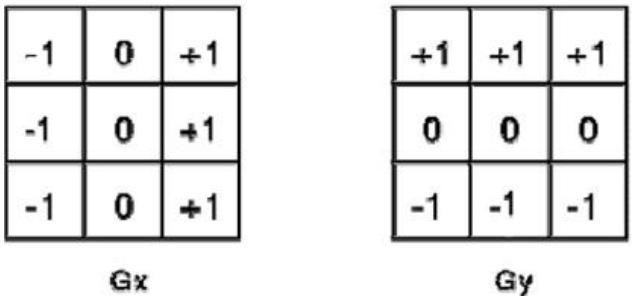

Figure 2.9 Prewitt operators

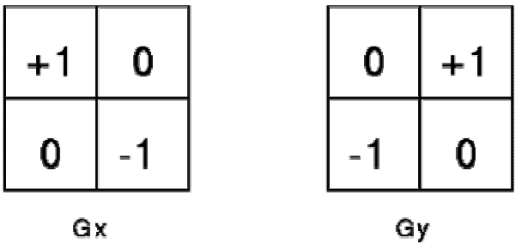

Figure 2.10 Roberts operators

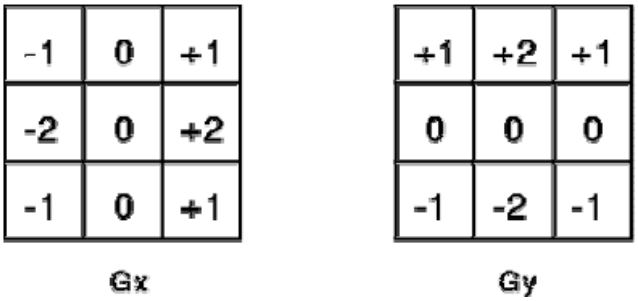

Figure 2.11 Sobel operators

The Canny operator works in a multi-stage process. First of all the image is smoothed by Gaussian filtering. Then a simple 2-D first derivative operator (somewhat like the Roberts Operation) is applied to the smoothed image to highlight regions of the image with high first spatial derivatives. Edges give rise to ridges in the gradient magnitude image. The algorithm then tracks along the top of these ridges and sets to zero all pixels that are not actually on the ridge top so as to give a thin line in the output, a process known as non maximal suppression. The tracking process exhibits hysteresis controlled by two thresholds: T1 and T2 with T1 > T2. Tracking can only begin at a point on a ridge higher than T1. Tracking then continues in both directions out from that point until the height of the ridge falls below T2. This hysteresis helps to ensure that noisy edges are not broken up into multiple edge fragments.

2.3.5 Morphological image processing [9]

Morphological image processing is used for extracting image components in order to represent and describe region shape, such as boundaries, skeleton, etc. It is also used for pro-processing and post-processing, such as morphological filtering, thinning and pruning. There are 4 basic operations as erosion, dilation, opening and closing. Erosion is used for shrinking the objects, while dilation is used for expanding the objects. To smooth the protruding points, break the narrow isthmuses or eliminate thin protrusions, opening operator is applied. On the other hand, closing is applied for smoothing intrusive points, fusing narrow breaks, filling the gaps within the objects or eliminating small holes.

2.4 Literature reviews

The automatic cephalometric landmark detection systems usually combine the knowledge about Image Processing, Artificial Intelligence and Machine Learning. Hence, we classify the automatic detection approaches into 5 general categories [10]: Hand-crafted approaches, Pattern Matching-based approaches, Model-based approaches, Artificial Intelligence-based approaches and combinations of several approaches.

As previously explained, the orthodontist first traces the lines of the lateral skull x-ray image, and then locates the landmarks referred to their definitions such as a junction of 2 lines, deepest points, protruding points, etc. The first attempts to automate cephalometric landmark detection system imitated the orthodontist's steps. These approaches are called as Hand-crafted Approaches. Since the most important task for this approach is edge detection, noise removal is the essential process. First research was started in 1986 by Levy-Mandel [11] Since Levy-Mandel's process took quite long time, three year later Parthasaratty [12] attempted to reduce processing time by applying a resolution pyramid technique. Many researchers tried to improve the success rate in this approaches. One of the best results in these approaches was done by Davis and Taylor in 1991 [13]. They used a blackboard architecture which integrated multiple problem solving modules.

Hand-crafted approaches are highly correlated to the quality of the images. Unfortunately, landmarks cannot all be located on significant edges. The system's algorithm is generally too rigid as it is difficult to add new rules to it. Therefore, there have been no more attempts to use the pure hand-crafted approaches thus far. It lead to the second category, pattern Matching-based Approaches. Researchers focus on how to match each landmark. The basic use of template matching algorithm is a mathematic morphology. In 1994, Cardillo [14] employed gray scale morphology operator, called "Gray-level Target Recognition Algorithm", and reported that the use of

only mathematic morphology could not locate all landmarks. Next in 2001, Grau [15] improved the system based on Cardillo's method by detecting the lines, followed by template matching. Laplacian of Gaussian (LoG) and zero crossing were employed for searching four reference lines. And then, landmarks were located by using template matching based on gray scale mathematic morphology. Beside mathematic morphology, Rudolph applied Spatial Spectroscopy method to classify and match pixels [16], [17]. Spatial spectroscopy is a method that decomposes an image by convoluting it with a set of filters. Their experiments on 2 filter sets, Multiscale Derivative and Offset Gaussian, showed that there were no significant differences between those 2 filter sets ($P > 0.05$). Compared with manual identification in low resolution, there were also no significant differences. However, the mean error on the original radiograph is significantly less than that on low resolution images. This indicated that the method should be improved and tested with higher resolution images.

The next approaches are model-based Approaches. Unlike the two previous categories, these approaches locate each landmark separately. There is no relationship between each landmark, while the methods in this category construct a model based on the hypothesis that there are some relationships between each point. Those points are from both real cephalometric landmarks and pseudo landmarks. There are two well-known model analyses, Active Shape Model (ASM) and Active Appearance Model (AAM). Active Shape Model is a statistical model of the shape of an object, while Active Appearance Model comprises both shape and texture variations. In order to define a model, it requires the mean shape and its variations, called Point Distribution Model (PDM). Principle Component Analysis (PCA) was used to reduce the high dimension of PDM. Hutton [18] and Yue [19] are researchers who applied ASM for locating cephalometric landmarks. Since only one model representing all points in ASM, the model is not flexible. Hutton's average recognition rate was only 35%. Yue customized ASM and combined with many techniques so that his recognition rate reached 71%. For Active Appearance Model (AAM), it was utilized in many researches

such as Sylvia [20], Predrag [21] and others. Sylvia also used top-hat operation, a kind of mathematic morphology, to extract low-contrasted components with respect to the background, and applied Principle Component Multivariate Linear Regression Model to generate new images which best fitted an unseen image. Predrag improved the system processing speed by applying AAM with pyramid resolution technique. Although, Predrag's recognition is better than Sylvia's, both are not better than the previous who used ASM. The model-based approaches tend to be time consuming since a large number of points must be labeled manually in the training stage. On the contrary, the larger the number of points is labeled, the more robust the model is. Therefore, a trading off between training time consumption and robustness of the model must be considered for this category.

It was noticed that all previous approaches were rule-based approaches. They lacked of flexibility. It was difficult and perhaps not suitable for identifying cephalometric landmarks because these landmarks varied among patients' skull structure. Many researchers shifted to apply Artificial Intelligence (AI) to gain more flexibility. Thus, this category is called Artificial Intelligence-based Approaches. Neural Network (NN) was firstly applied. It consists of an input layer, hidden layer(s) and an output layer. In each layer, there are nodes which connect to the next layer by weighting. The algorithm updates each node's weight iteratively and stops when the output error falls within the specified error range. The size of the input pattern is an important factor in NN performance. Larger input patterns accrue additional computation costs. Moreover, it is not helpful for generating feature extraction. On the other hand, smaller input patterns might cost less but possibility of errors increases. Again, a trade off between computation costs and accuracy is a point for consideration when constructing such system. Another AI-based algorithm is Genetic Algorithm (GA). The strongest sample that can survive throughout the selection process is the best answer. GA is good for speeding up the process. It is helpful in accelerating the function convergence. In 1999, Chen [22] used NN with GA to extract features of sub images.

The algorithm was tested with 9 landmarks. The accuracy of detect landmark in sub images was 84% (NN without GA) and 94 % (NN with GA). In 2003, Ciesielski [23] used only GA to detect landmarks. For the training dataset, they manually specified square regions centered by each landmark. These square regions must contain enough information that can distinguish each landmark. In the recognition stage, they used GA to locate the landmarks. There were also many attempts using NN such as Innes [24], El-Feghi who applied NN in different ways [25], [26], [27], [28]. Unlike NN and GA which are not statistical algorithms, Support Vector Machine (SVM) is. It is for classification and more reliable than NN and GA. Chakrabarty [29] extracted Projected Principle-Edge Distribution (PPED) feature in 4 directions as the input for SVM to classify landmarks.

Since rule-based approaches are quite rigid and AI-based approach is too general, a combination approach might provide better results. Moreover, trying to match landmarks without approximate locations is time consuming and usually gets false alarms (unnecessary alarms to a place where they are not needed). Referring to Mohseni [30], general methods could be used for estimating initial landmark locations, but not for exact localization purposes. Thus, they approximated the location of each landmark by using knowledge-based methodology. Projection profiles were used to find the regions of interest. The choice of method to localize landmarks depended on the landmarks' characteristics. Edge enhancement was suitable for landmarks which were on significant edge, while template matching was for landmark which possessed special characteristic information. The average error of this research was quite high, 93% (8 landmarks). The latest work in this category was Rahele et al. in 2007 [31]. Although, they employed many processes such as non linear diffusion, Susan edge detection, opening mathematic morphology, K-means clusters, Learning Vector Quantization Neural Network (LVQ NN), multi-resolution method, ASM, and pattern matching algorithm, the average recognition rate is about 61% (16 landmarks).

CHAPTER III

Methodology

This chapter firstly describes overview of our methodology, and algorithms used in our work to detect each landmark step by step.

3.1 Overview

Our methodology divides into 2 main stages as training stage and recognition stage as shown in Figure 3.1. Training stage combines image processing technology and statistical model to generate models and their SDs. The general models and their SDs are employed in recognition stage to specify ROI and locate cephalometric landmarks then.

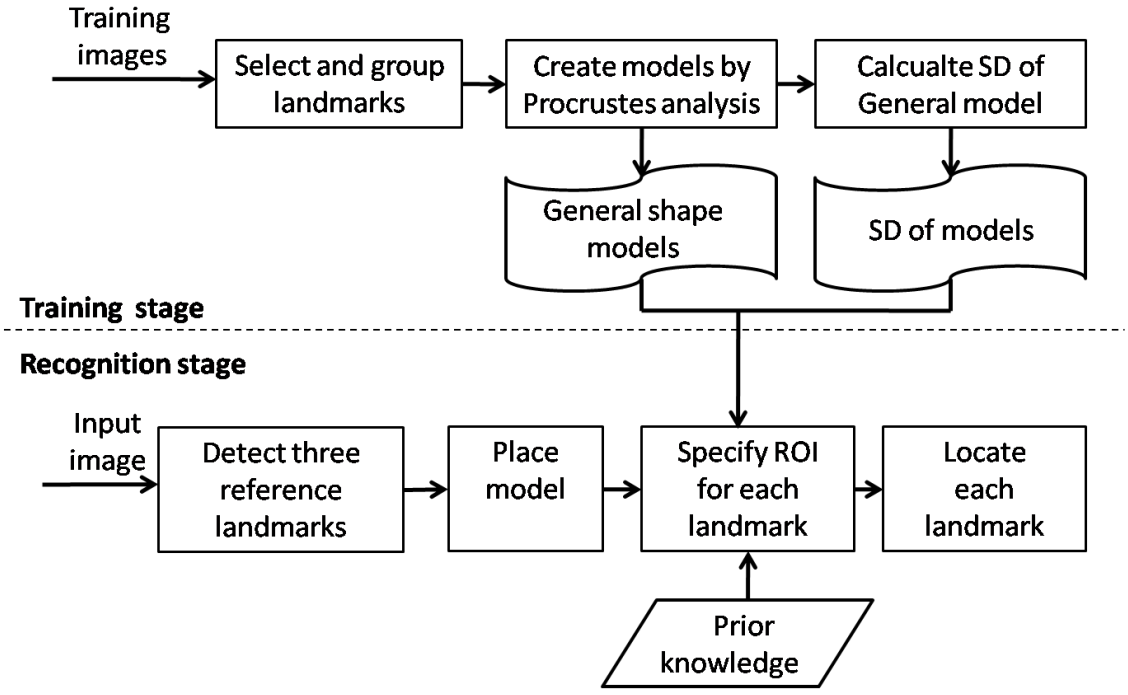

Figure 3.1 Methodology flowchart

First of all, we select a set of landmarks as our experiment landmarks and group them into 2 groups as upper and lower face structure. For each structure, Procrustes analysis is used to create general models. Finally, the standard deviation for each landmark is calculated from general model. When an input sample comes, 3 reference landmarks are first detected by image processing. Then, the general models are placed referred to those 3 landmarks. Region of interest (ROI) of each landmark is specified related to the general model and each SD. Finally, landmarks are located using prior knowledge and image processing methodology.

3.2 Select and group landmarks

As explained above, only 19 of those 40 landmarks are applied in the first orthodontic analysis as shown in Table 3.1. Apparently, 16 out of those 19 landmarks are on bone structure, and the rest, on soft tissue. Table 3.1 illustrates the landmark name, location and number, as referred to in figure 2.1.

As mentioned earlier, our method is to select only the landmarks on the bone structure. Moreover, we exclude some landmarks which are intra-oral landmarks; as number 7, 8, 9 and 14, and detail landmarks; as number 18. Thus we choose land marks numbers ***1-3, 5-6, 13, 15, 17, 19-20 and 23*** to create our facial structure model.

Since the landmarks on the lower part may widely vary from one head to another, especially around the teeth and lips, while those on the upper part are more alike, we therefore separate those 11 landmarks into 2 groups as upper and lower part. Moreover, we add two more points to our upper and lower models. They are the Ear-rod and ANS (the most anterior point on the maxilla which is marked as number 4 in figure 2.1). The reasons are as follows: Firstly, Ear rod, which is an instrument to fix every patient's face position, can be clearly identified in every patient's x-ray image. Secondly, ANS is located on the middle line of a face [2]. Hence it is a good reference for dividing the head into two parts, the upper and the lower.

Table 3.1 Cephalometric landmarks in the first orthodontic analysis

(Number is related to figure 2.1 and figure 2.1)

No.	Landmark name	Location
1	Sella (S)	Bone
2	Nasion (Na)	Bone
3	Orbitale (Or)	Bone
5	Subspinale (A)	Bone
6	Incisor superius (Is)	Bone
7	Upper incisor apex (UIA)	Bone
8	Intersection of upper and lower first premolar	Bone
9	Intersection of upper and lower first molar	Bone
13	Incisor inferius (Ii)	Bone
14	Lower incisor apex (LIA)	Bone
15	Supramentale (B)	Bone
17	Pogonion (Pg)	Bone
18	Gnathion (Gn)	Bone
19	Menton (Me)	Bone
20	Gonion (Go)	Bone
23	Porion (Po)	Bone
30	Pronasion (Prn)	Soft tissue
36	Labrale inferius (Li)	Soft tissue
37	Soft tissue Pogonion (Pg')	Soft tissue

3.3 Create models by Procrustes analysis

We apply Procrustes analysis separately with upper and lower part structure.

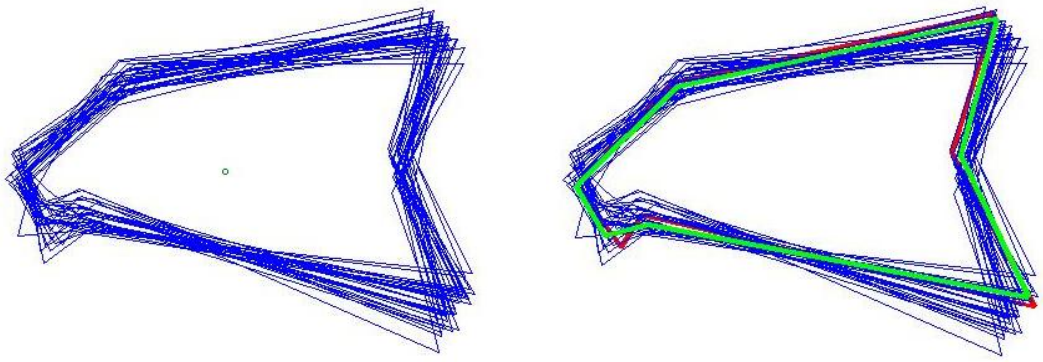

(a)

A set of prepared normalized shapes aligned by each centroid

(b)

All aligning shapes (blue lines) are aligned with the previous mean shape (red line) to approximate a new mean shape (Green line).

Figure 3.2 Procrustes analysis mean shape

3.4 Calculate SD of general model

In this research, we specify our ROI for individual point to be a rectangular centered at the model's point, of sized +/-2SD (Standard Deviation.) The SD is computed from each set of corresponding training points and the mean shape point. In order to compare shapes, the center of the line between the two fixed reference points in each shape must be aligned at the same position. The SD of each landmark is then calculated.

Each landmark's SD is obtained as follows:

1. Normalize each original shape by its centroid size.
2. Translate all shapes' centroids to the origin.

3. Use the line between the two fixed reference points as a reference line as shown in figure 3.4 (a)

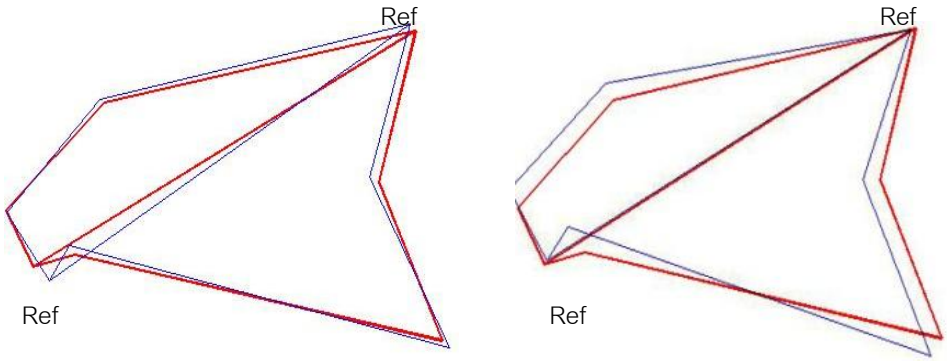

(a) shapes with line between the two fixed reference points. Red line for mean shape and blue line for an original shape;

(b) rotate and translate each shape corresponding to the line

Figure 3.3 Shape alignment for ROI specification

4. Calculate the angle of the reference line with respect to a horizontal line. Rotate each shape to this angle, and then translate the centers of the reference lines to the same position as that of the mean shape as shown in figure 3.4 (b)

5. Calculate a SD for each landmark by using the mean shape's position as the mean ($\bar{x}, \bar{y}$) of all corresponding points by Equation 3.1

$$SD_x = \sqrt{\frac{\sum(x_i - \bar{x})^2}{n}} \qquad SD_y = \sqrt{\frac{\sum(y_i - \bar{y})^2}{n}} \tag{3.1}$$

n: number of images
$(\bar{x}, \bar{y})$: coordinate of each landmark in mean shape

3.5 Pre-processing of recognition stage

Pre-processing is to prepare the input image to be ready for other processing. When the input image comes, to avoid the illumination error of image margins, 4 borders of image are trimmed. Due to our image acquisition is scanning an x-ray, there should be some noise. We assume that noise as random noise and reduce it with Gaussian filter. To create Gaussian filter, sigma (or standard deviation of Gaussian distribution) has to be defined. Our sigma is calculated by the area of image background as shown in Figure 3.4. The result image and its histogram from pre-processing are shown in Figure 3.5. Notice that histogram of filtered image is smoother than original's.

Figure 3.4 The area of image background
used for calculating SD of Gaussian distribution

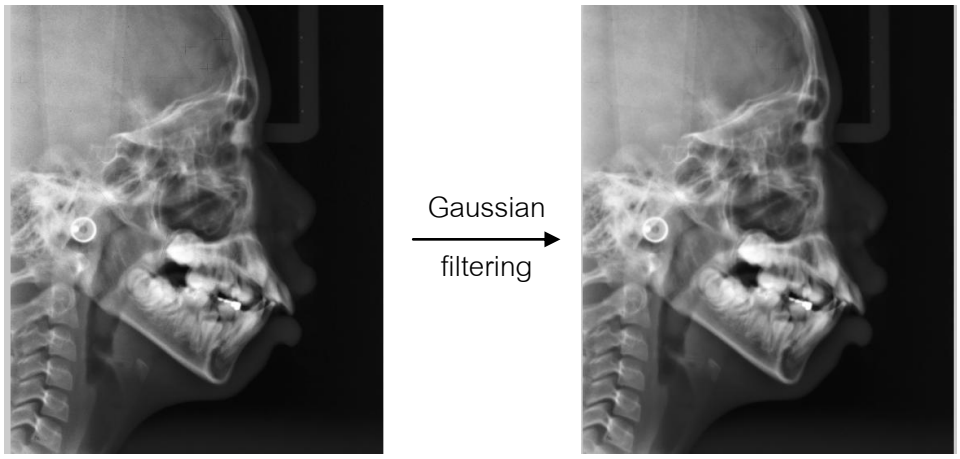

(a) Original image (b) Gaussian filtered image

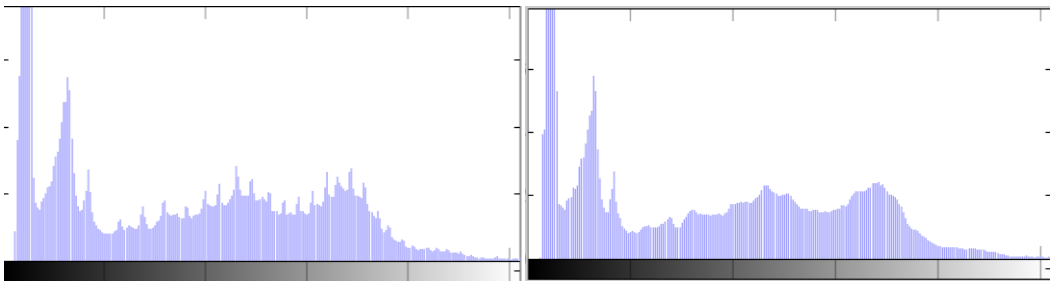

(c) Histogram of original image (d) Histogram of filtered image

Figure 3.5 Result of pre-processing

3.6 Detect 3 reference landmarks

We choose Ear rod, Nasion and Menton as reference landmarks for model placement. Menton are located first as the lowest point of face. Then, the border of structure is scoped. Referred from prior knowledge, approximate area of Ear rod and Nasion are defined. Finally, Ear rod and Nasion are located based on edge detection.

3.6.1 Histogram specification is applied to adjust histogram be as the desired shape. It makes all images in dataset have the similar histogram. First step is to select the target image. Since we aim to segment bone structure out of soft tissue and background, we choose image that its contrast between bone and other are obviously different (see Figure 3.6 (b)). The results are shown in Figure 3.6.

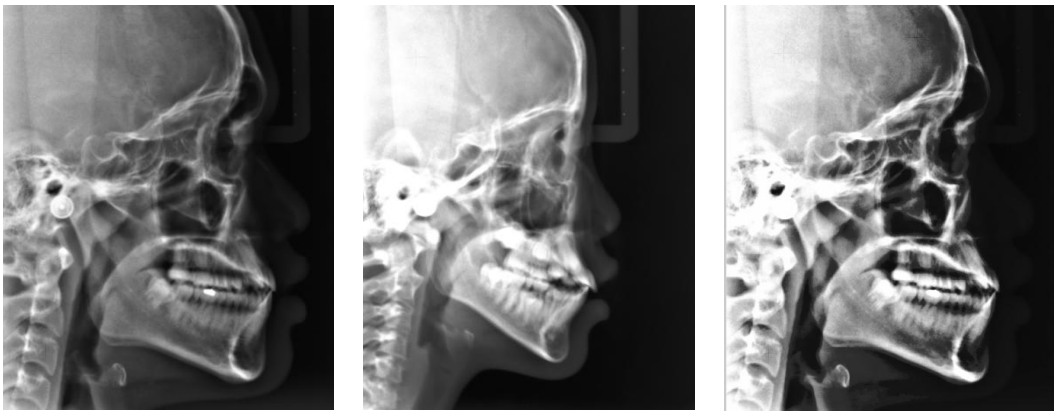

(a) Input image (b) Target image (c) Input image which passed histogram specification

Figure 3.6 Histogram specification results

3.6.2 Otsu thresholding is then applied in order to segment bone area. Since all images already have the similar histogram, the thresholing value is the same for all images. The results are shown in Figure 3.7.

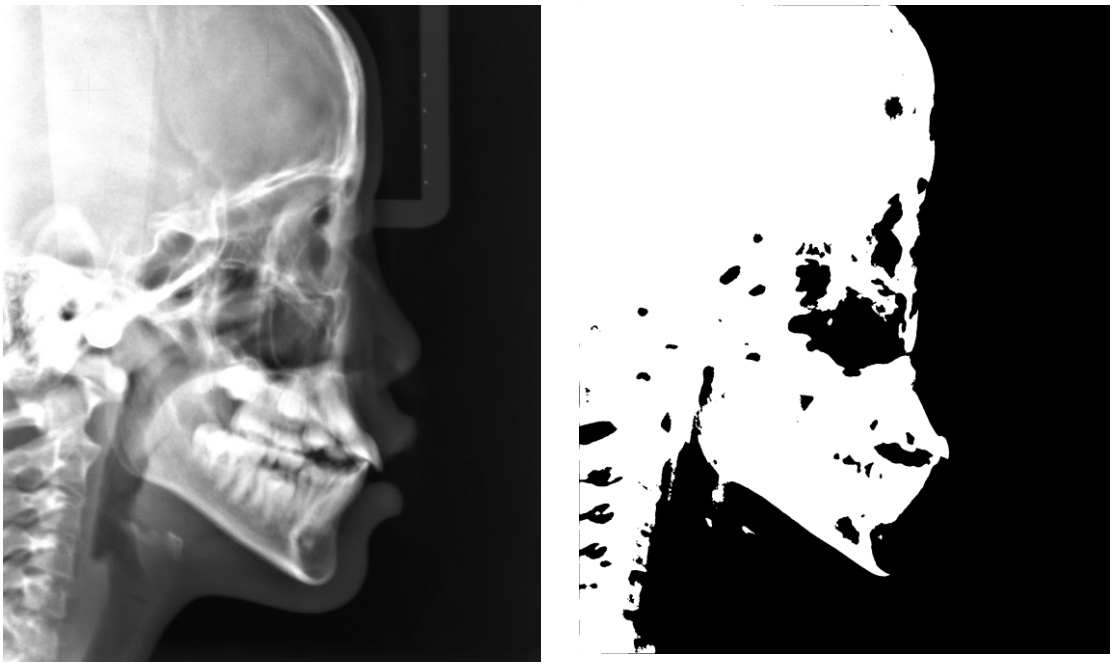

(a) Image passes histogram specification (b) Image passed Otsu thresholding

Figure 3.7 Otsu thresholding

3.6.3 After gray image turn into binary image, in order to clean remaining noise, opening morphology is applied. The result is smoother. Gaps and holes are filled.

3.6.4 Trace the boundary of lower face structure by scanning for the first white pixel horizontally from right to left on half lower part as shown in Figure 3.8. Then, we trace along the line to find *Menton* which is the lowest point. We also obtain the right boundary of face structure from the right-most point of the line.

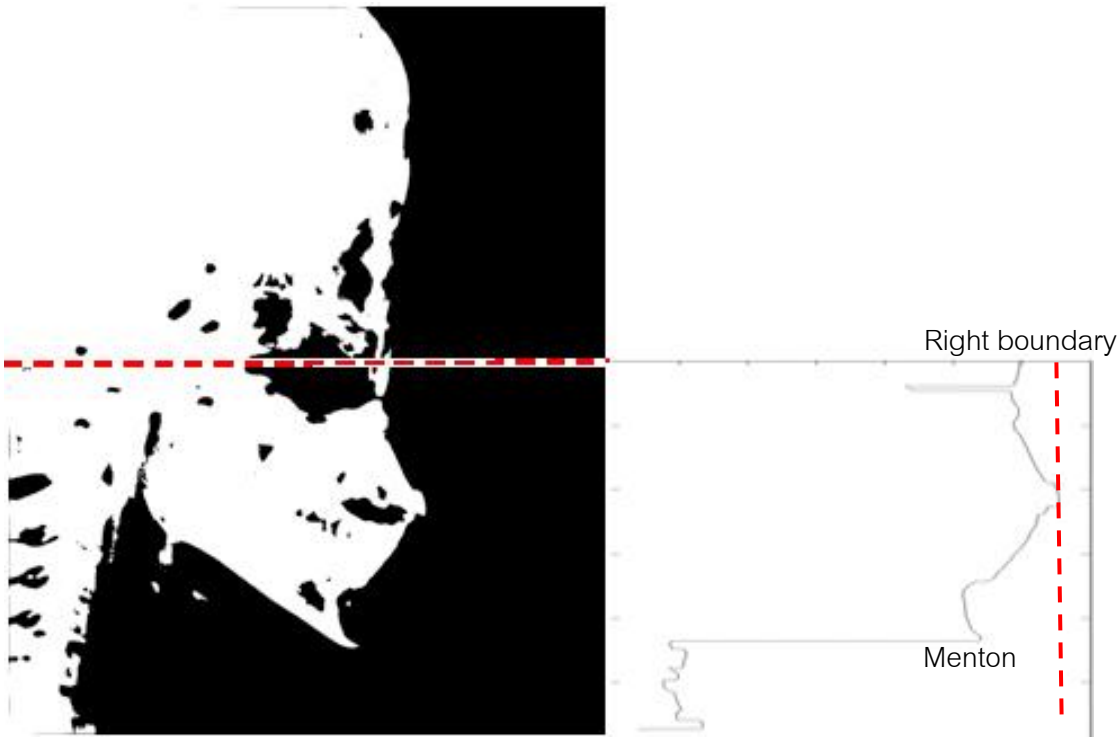

Figure 3.8 Result of line scanning

3.6.5 Next landmark is Ear rod. It always locates around the middle line of the image, back part of head structure which related to the right boundary from the previous step (see Figure 3.9 (a)). Figure 3.9 (b) is the ROI of ear rod. Then, Canny edge detection is applied to the ROI, the result is shown in Figure 3.19 (c). Finally, Circle

hough transformation is applied with various radius size (Figure 3.9 (d)). Ear rod is located at the location that has maximum value of hough transformation (Figure 3.9 (e)).

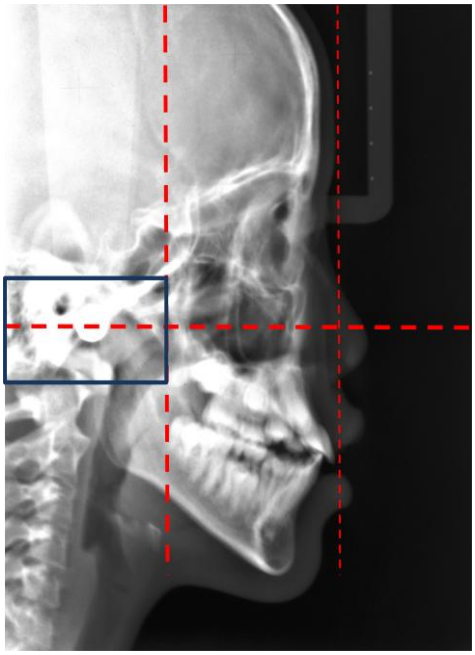

(a) Scope area for ear rod

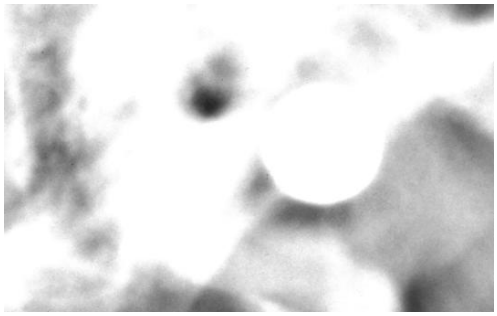

(b) ROI of Ear rod

(c) Canny edge detection

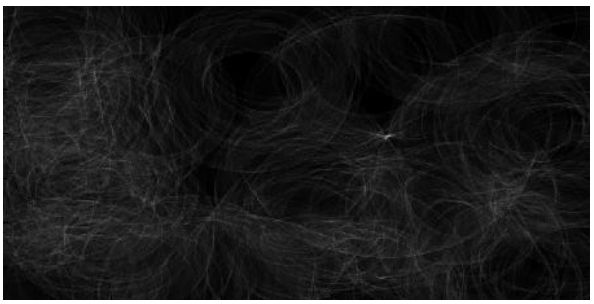

(d) Circle hough transform

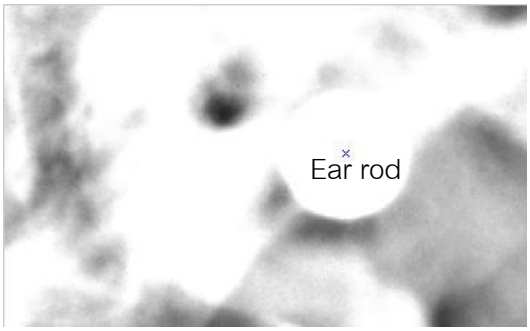

(e) The location of maximum value from circle hough transform

Figure 3.9 Ear rod detection

3.6.6 The last reference landmark is Nasion. It is located at the most top of our landmarks. Thus, we start to detect orbital pointer, a dental instrument which contacts near Nasion point, by edge detection. We scan horizontally from right to left on the top of the image to find the second line of the dental instrument. Then, we trace a line of the instrument until it ends at soft tissue. Bone structure is the later line from soft tissue, so we choose the later line, and trace along that line to find an intersection point which is Naion (see Figure 3.10).

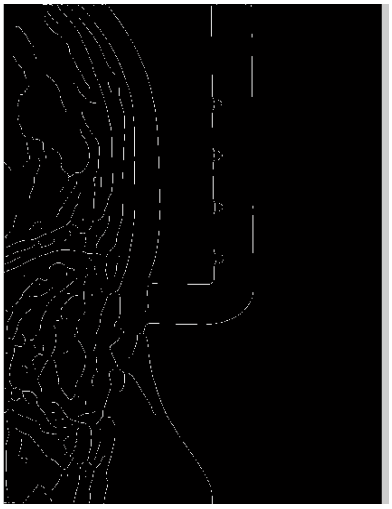

(a) Canny edge detector with a right quarter part of image

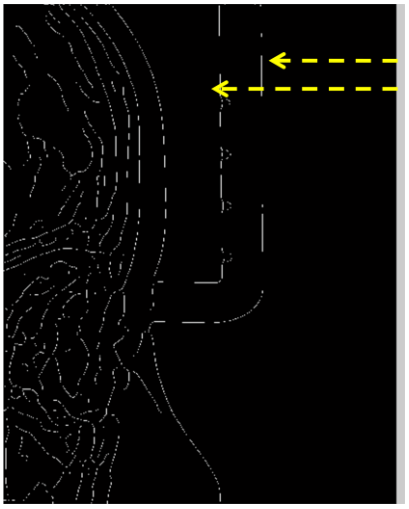

(b) Horizontal scan to find the second line of orbital pointer

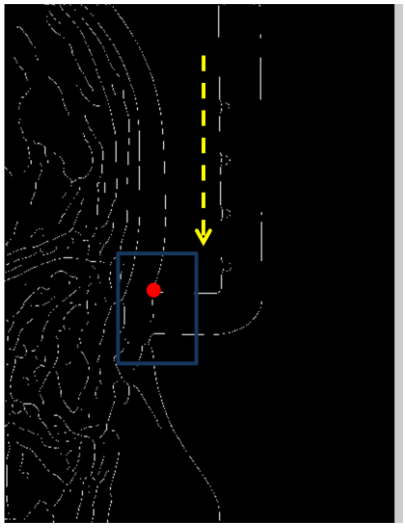

(c) Trace the line until end at soft tissue

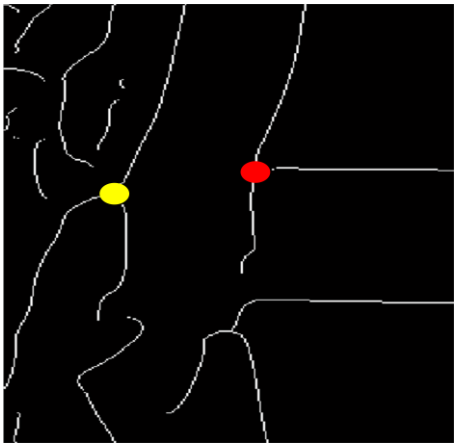

(d) Find the

Figure 3.10 Nasion detection

3.7 Place model using 3 reference landmarks

We place our general model separately upper and lower part. For upper part, we use Ear rod and Nasion as reference points. The model is aligned into the line of Ear rod and Nasion. The result is shown in figure 3.11. For lower part, we use Ear rod and Menton as reference points, and do the same alignment. The result is shown in figure 3.12.

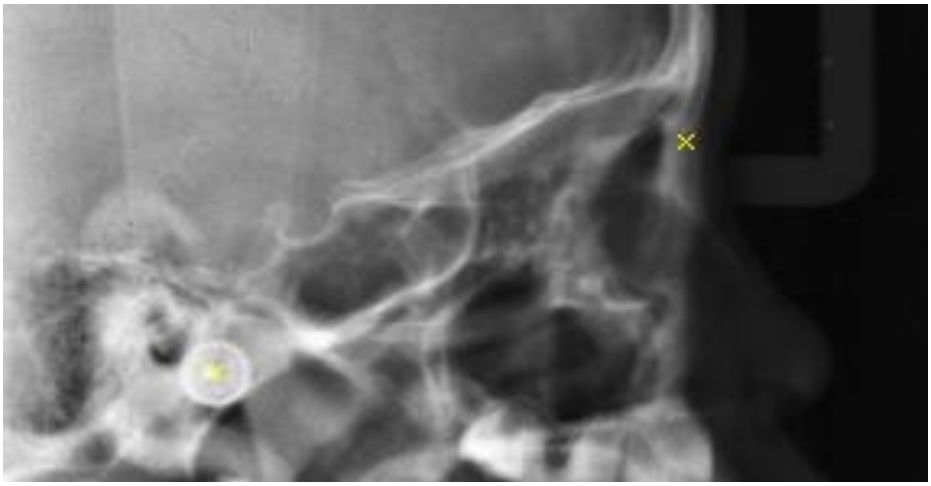

(a) The result from Ear rod and Nasion detection

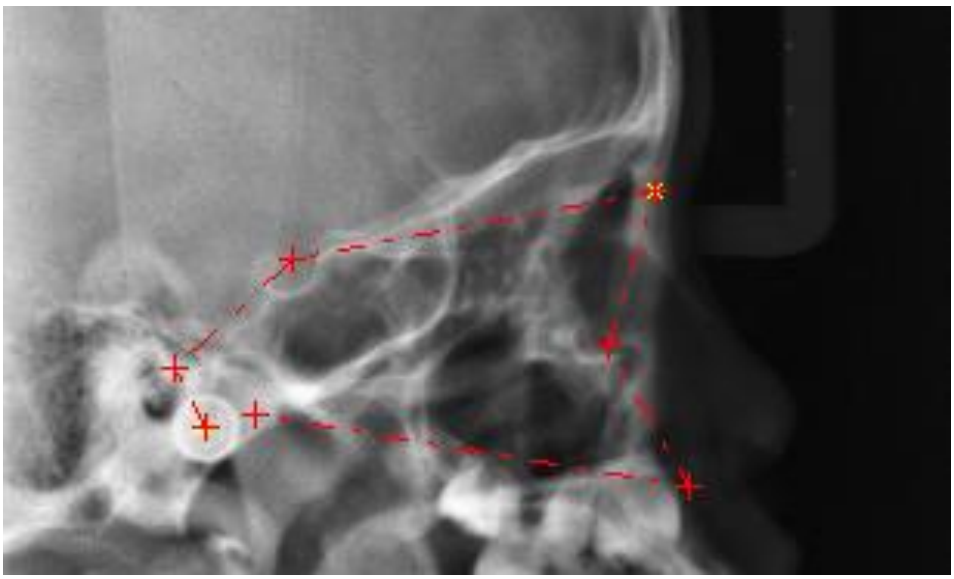

(b) Upper model placement

(alignment with the line of Ear rod - Nasion)

Figure 3.11 Upper model alignment

(a) The result from Ear rod and Menton detection

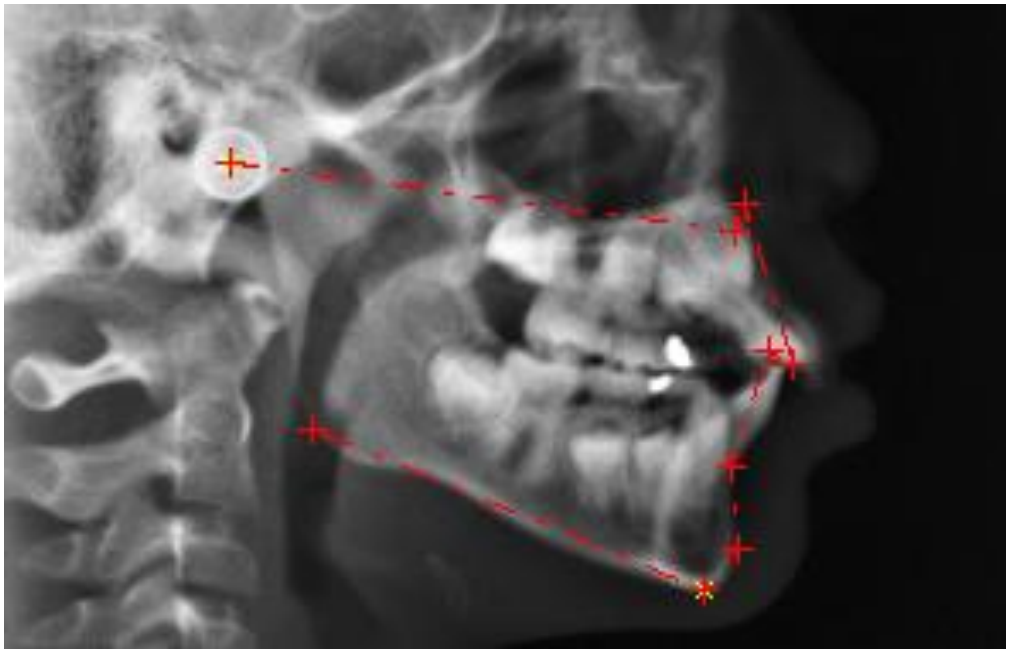

(b) Lower model placement

(alignment with the line of Ear rod – Menton)

Figure 3.12 Lower model alignment

3.8 Specify ROI for each landmark

We specify the region of each landmark after model placement by expanding the area from the location of each landmark. The ROI is considered from SD of each landmark and anatomical knowledge. Figure 3.13 (a) show ROI of each landmark on upper part of face, while Figure 3.13 (b) is for the lower part.

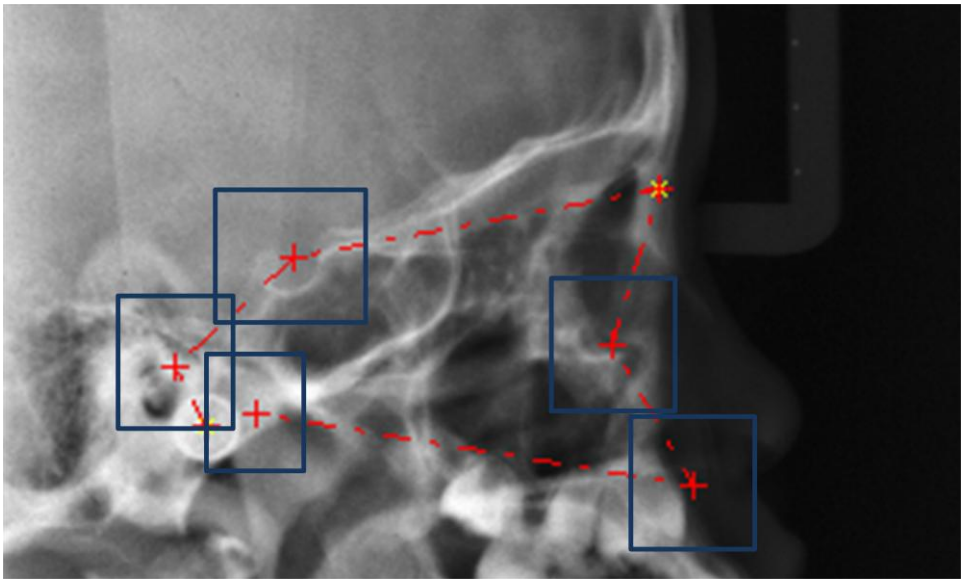

(a) ROI on upper part

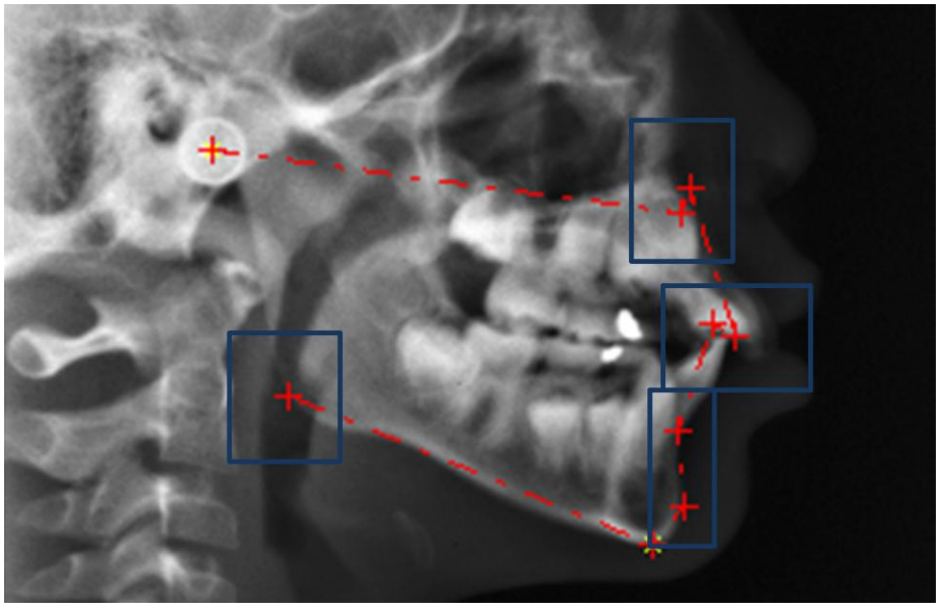

(b) ROI on lower part

Figure 3.13 ROI of each landmark

3.9 Locate each landmark

3.9.1 Porion: Due to its shape which is like half of a circle, circle hough transformation is applied in ROI after local pre-processing (see Figure 3.14).

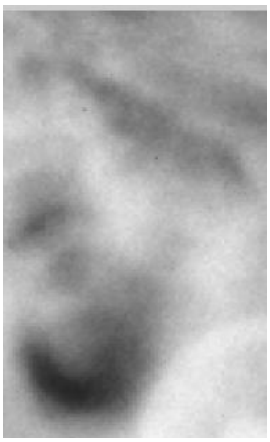

(a) ROI of Porion

(b) Otsu threshodling

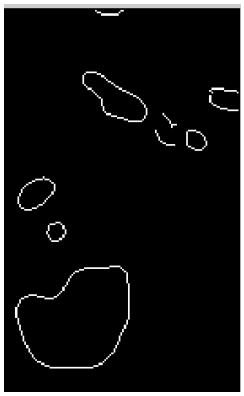

(c) Canny edge detection

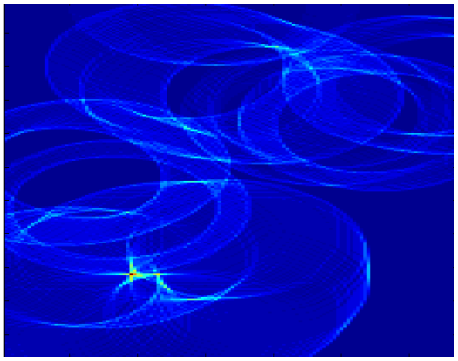

(d) Circle hough transformation

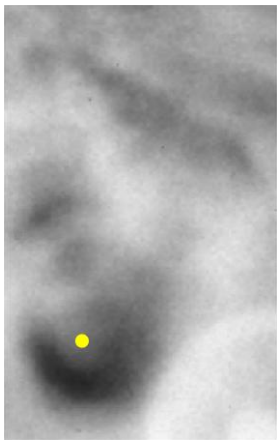

(e) Location from circle hough transformation

Figure 3.14 Porion detection

3.9.2 Sella: Due to its shape which is like half of a circle, Circle hough transformation is also applied in ROI after local pre-processing (see Figure 3.15).

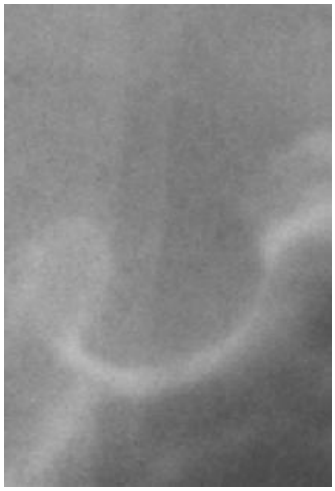

(a) ROI of Sella

(b) Canny edge detection

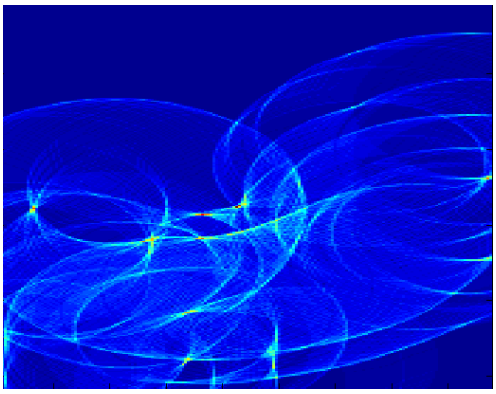

(c) Circle hough transform

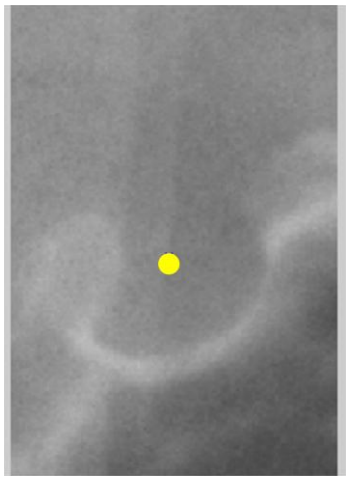

(d) Location form circle hough transform

Figure 3.15 Sella detection

3.9.3 Orbitale: It is the most protruding point of bone in the ROI. Thus, thresholding is applied to convert gray image into binary image. Then, find the most-right point (see Figure 3.16).

3.9.4 ANS: It is the most protruding point of bone locating in the middle line of head structure. ROI is considered from the model location and also Ear rod location. Thresholding is applied with ROI, and then ANS is located as the protruding point (see Figure 3.17)

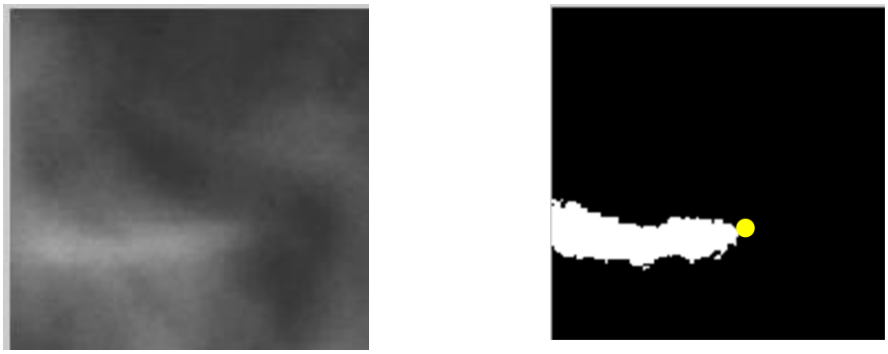

(a) ROI of Orbitale (b) Canny edge detection

Figure 3.16 Orbitale detection

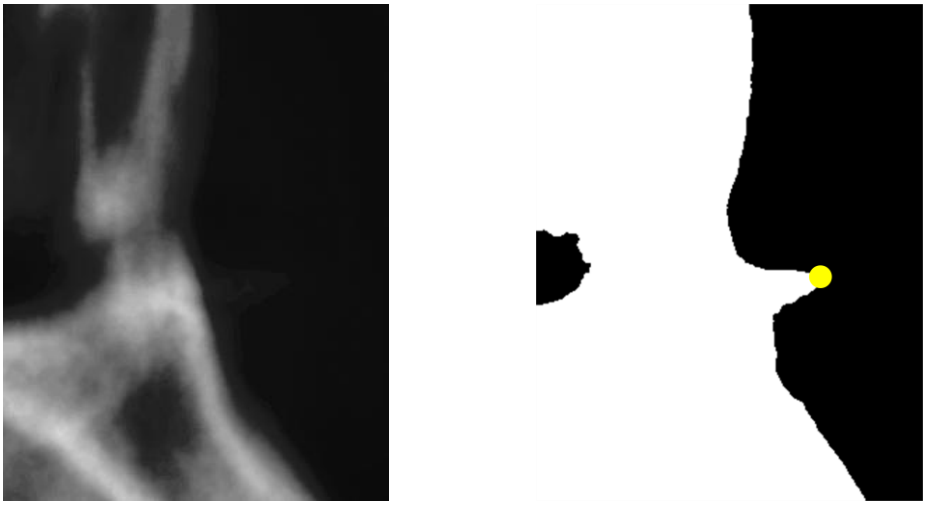

(a) ROI of ANS (b) Thresholding

Figure 3.17 ANS detection

3.9.5 Subspinale: It is deepest point on the contour between the spinal point and prosthion. According to this point relate to ANS, the location of ANS is considered as a scope of Subspinale. As same as ANS, thresholding is applied with ROI, and then Subspinale is located as the deepest point under ANS (see Figure 3.18)

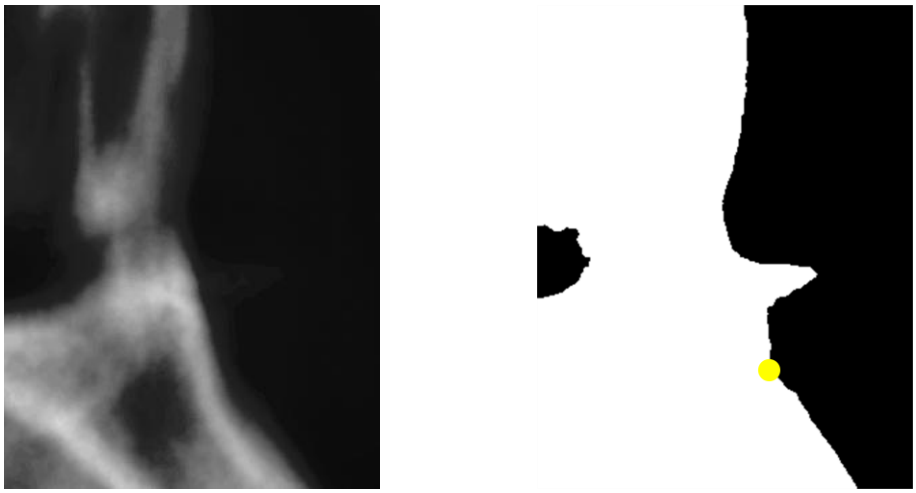

(a) ROI of Subspinale (b) Thresholding

Figure 3.18 Subspinale detection

3.9.6 Incisor superius and Incisor inferius: It is the incisal tip of the most antertior maxillary and the most labial mandibular central incisor, respectively. We expand the area around mean-shape location. Canny edge detection is applied in the ROI. Scan image horizontally to find the first line. On the upper part of ROI, we trace down the line to the end of the line to locate Incisor superior. And on the below part of ROI, we also trace up the line to end of the line to locate Incisor inferior (see Figure 3.19)

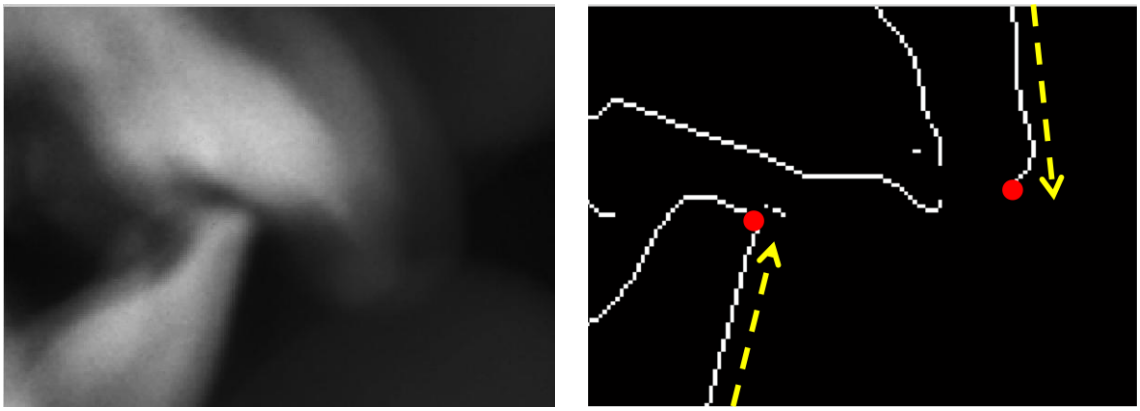

(a) ROI of Incisor superior and inferius (b) Canny edge detector and trace the line to the end of the line

Figure 3.19 Incisor superior and inferius detection

3.9.7 Supramentale and Pogonion: Due to menton is the lowest point of the head structure, it is used as the lower border of ROI. The upper border is related to mean shape location. We define line to divide searching for Supramentale and Pogonion by average value of upper border line of Pogonion and lower border line of Supramentale. For upper part of the dividing line, we search for the most concave point to be a Supramentale. On the other hand, we search for the steepest point in the lower part of the dividing line to be a Pogonion (see Figure 3.20).

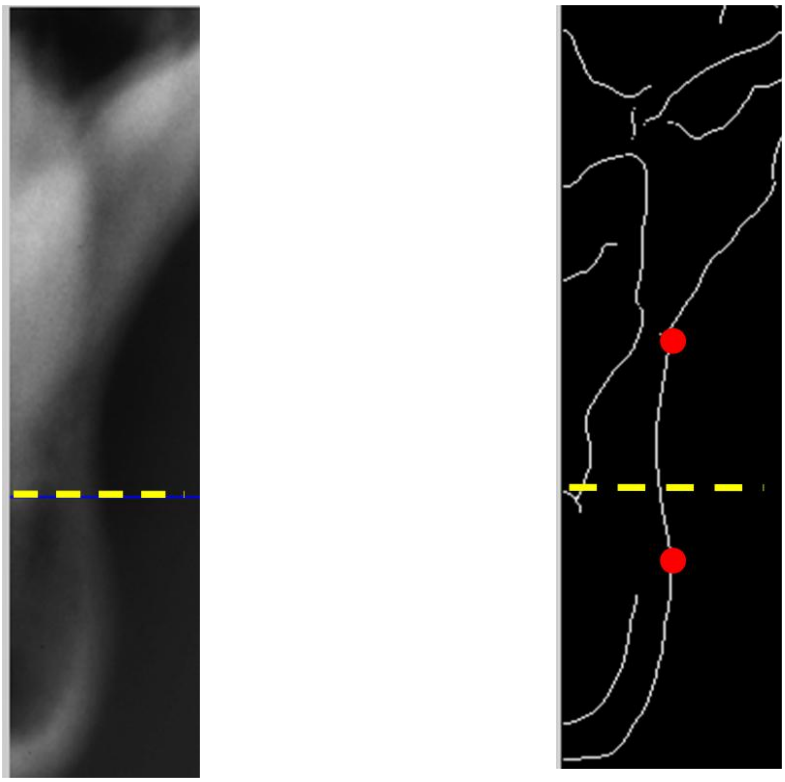

(a) ROI of Supramentale and Pogonion (b) Canny edge detector and trace the line

Figure 3.20 Supramentale and Pogonion detection

3.9.8 Gonion: To find Gonion, we start from creating a guide line from Menton upward (see Figure 3.21 (a)). From model placement, ROI is defined as area centered its location with +/- 3SD (see Figure 3.21(b), and then it is applied with Canny

edge detection (see Figure 3.21(c)). We trace the line which has the similar slope and nearby location with the guide line (see Figure 3.21(d)). Gonion is located about the middle of the line which has an angle between the guide line and itself within a threshold (see Figure 3.21(e)).

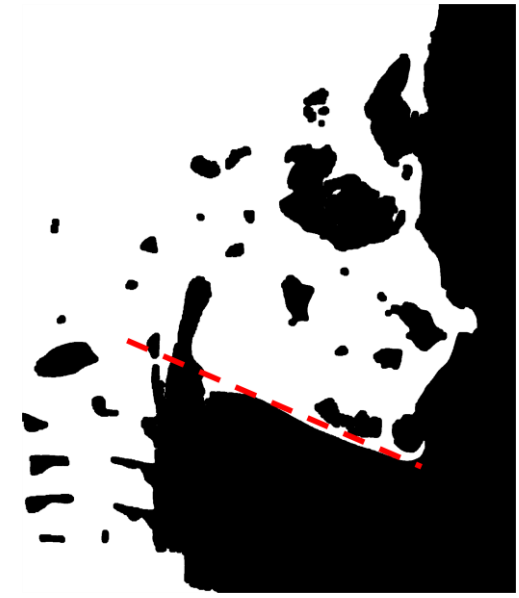

(a) Create a line from Menton upward

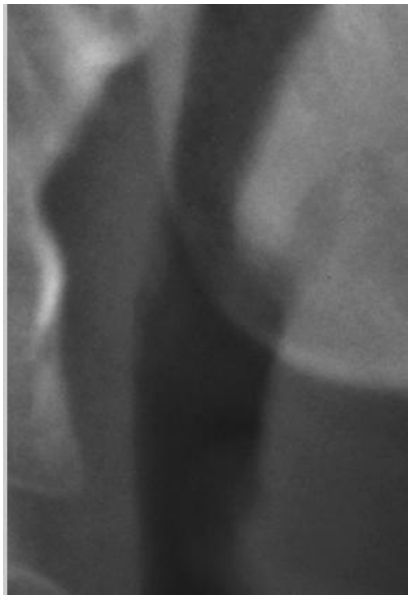

(b) ROI of Gonion

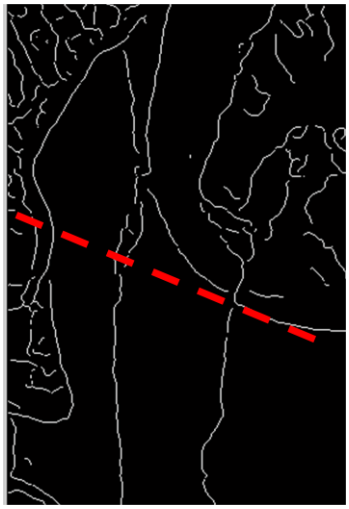

(c) Canny edge detection

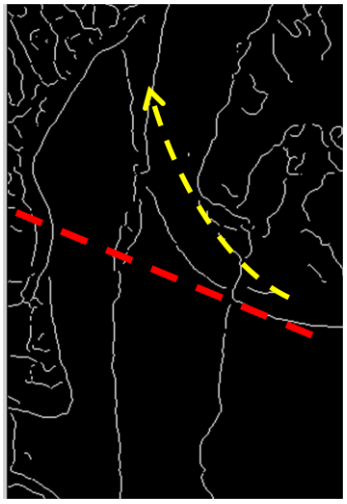

(d) Trace the line by considering the angle of the line

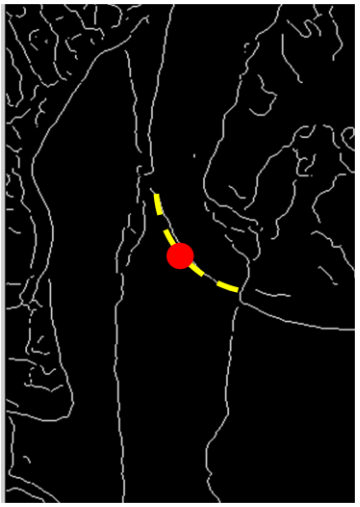

(e) Trim the line. Only the line which has angle within a threshold left.

Figure 3.21 Gonion detection

CHAPTER IV

Experiments and Results

This chapter describes about our materials, tools, and how we designed and evaluated our experiment.

4.1 Materials

Thirty cephalograms, scanned with 300 dpi, have been used in our experiments. The length in the scanned image is converted with scanning resolution rate. Hence, the size of one pixel in the scanned image is 1/300 inch or 25.4/300 mm. or 0.0847 mm. Patients' ages are in range of 8 – 42 years old. An example is shown in Figure 4.1.

Figure 4.1 A cephalometric radiograph used in the thesis

All the landmarks in 30 x-ray images used in this research have been manually specified by an orthodontic expert. Each image contains 13 landmarks; 11 from the first orthodontic analysis and the Ear-rod and the ANS.

4.2 Computer specification and tools

In this study, we performed the experiments on an operating system Windows 8 64-bit on ACER workstation with Intel core i3-3228U CPU @ 1.90 GHz and 8 GB of memory. For coding, we used C# programming language to connect with Microsoft SQL Database server 2008 Express for data retrieving, and used MATLAB 7.10.0 (R2010a) (Educated license) for implementation.

4.3 Evaluation

To evaluate our algorithms, an expert was firstly evaluated by Dahlberg's formula, which calculates an intra-observer error. Next, our +/-2SD models were measured the success rate. And finally, we compared our method error with an intra-observer error.

4.3.1 Evaluate an expert (Intra-observer error)

There are two sets of manually located landmarks in our study. An expert orthodontist was asked to mark a set of landmarks in ten cephalogram images. Two weeks later, the same orthodontist was asked to redo the work. The first set of manually located landmarks is used as our ground truth, and the second set reveals the intra-observer error by calculating Dahlberg's formula [32], as shown in equation 4.1

$$D = \sqrt{\frac{\sum_{i=1}^{N} {d_i}^2}{2N}} \tag{4.1}$$

N: number of images
d : distance between two times marking

Table 4.1 Intra-observer error calculated by Dahlberg's formula

Landmark name	Absolute distance error		
	Horizontal (mm.)	Vertical (mm.)	Euclidean (mm.)
Ear rod	0.09	0.09	0.13
Porion	0.34	0.72	0.80
Sella	0.13	0.20	0.24
Nasion	0.24	0.40	0.47
Orbitale	0.77	0.22	0.80
ANS	0.57	0.36	0.68
Subspinale	0.40	0.39	0.55
Incisor superior	0.16	0.30	0.35
Incisor inferior	0.24	0.19	0.30
Supramentale	0.30	0.67	0.74
Pogonion	0.22	0.58	0.62
Menton	0.33	0.13	0.35
Gonion	0.57	0.73	0.93

* calculated from 10 images

Table 4.1 shows errors which are calculated by Dahlberg's formula. Since Ear rod is an instrument, it is excluded from intra-error report. For horizontal, Orbittale is the maximum error landmark, while Sella is the minimum error landmark. For vertical, Gonion is the maximum error landmark, while Menton is the minimum error landmark. For Euclidean distance, Gonion is the maximum error landmark, while Sella is the minimum error landmark. However, intra-observer errors are all less than 1 mm. which means our clinician is accurate and precise.

4.3.2 Evaluate the general models

After training stage, we got two general models of the upper and the lower part with its SDs. Thus, we testes out models what the success rate of finding cephalometric landmark in ROI. We defined ROI as a rectangular centered at the model's point, of sized +/-2SD (Standard Deviation). Leave-one-out algorithm was employed. Based on the number of our dataset, 30 cephalograms, it means we split one data set for testing and the remaining 29 cephalograms for creating our general models. The results were reported in our publication [33] as shown in Table 4.2.

Table 4.2 Success rate of finding cephalometric landmark in ROI (+/-2SD)

	Landmark name	No. of matched results (out of 30)	Success rate (%)
Upper Model	Sella	26	86.67
	Orbitale	24	80.00
	ANS	26	86.67
	Porion	27	90.00
		Average	**85.84**
Lower Model	ANS	25	83.33
	Subspinale	23	76.67
	Incisor Superior	23	76.67
	Incisor Inferior	23	76.67
	Supramentale	26	86.67
	Pogonion	30	100
	Gonion	25	83.33
		Average	**83.33**

From Table 4.2, It shows that the average success rates of finding Cephalometric landmarks in the +/-2SD ROI's in the upper and the lower parts are both good at over 80%. It also means many landmarks will be misses if used only this constraint.

4.3.3 Comparison our error with Dahlberg's formula

In order to be consistent with intra-observer error measurement, our results were compared with ground truth to find absolute error distance. Dahlberg's formula was applied with N = 30.

Table 4.3 Our results error calculated by Dahlberg's formula

Landmark name	Our results (30 images)			Intra-observer (10 images)		
	Horizontal (mm.)	Vertical (mm.)	Euclidean (mm.)	Horizontal (mm.)	Vertical (mm.)	Euclidean (mm.)
Ear rod	0.06	0.08	0.10	0.09	0.09	0.13
Porion	1.29	2.37	2.70	0.34	0.72	0.80
Sella	1.77	2.75	3.28	0.13	0.20	0.24
Nasion	0.27	1.01	1.04	0.24	0.40	0.47
Orbitale	1.47	0.80	1.67	0.77	0.22	0.80
ANS	0.62	0.18	0.65	0.57	0.36	0.68
Subspinale	3.04	1.45	3.37	0.40	0.39	0.55
Incisor superior	2.28	1.24	2.60	0.16	0.30	0.35
Incisor inferior	1.53	0.71	1.68	0.24	0.19	0.30
Supramentale	0.33	0.69	0.77	0.30	0.67	0.74
Pogonion	0.17	0.45	0.48	0.22	0.58	0.62
Menton	0.36	0.27	0.46	0.33	0.13	0.35
Gonion	1.57	1.36	2.07	0.57	0.73	0.93

Ear rod is excluded from the report. For horizontal, Subspinale is the maximum error landmark, while Nasion is the minimum error landmark. For vertical, Sella is the maximum error landmark, while Menton is the minimum error landmark. For Euclidean distance, Subspinale is the maximum error landmark, while Menton is the minimum error landmark. There is only Ear rod, whose error from our results is less than intra-observer error.

4.3.4 Our results error calculated by Dahlberg's formula

Besides of an absolute error distance, we also considered the direction of errors as shown in Figure 4.2.

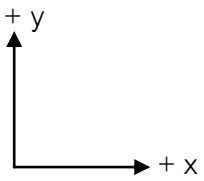

Figure 4.2 Direction of errors

Table 4.4 shows Minimum, maximum and mean distance error of our results. We can categorize our results into 3 groups of error distance. First group is a set of landmarks whose errors are less than 3 mm. There are Ear rod, Nasion, ANS, Incisor superior, Incisor inferior, Supramentale, Pogonion and Menton. The second group is a set of landmarks whose errors are more than 3 mm but less than 5 mm. There are Sella, Orbitale, and Subspinale. And the last group, landmark errors are more than 5 mm. There are Porion and Gonion.

We also show the detail of errors for each landmark. The detail of intra-observer error shows in Appendix A, and in appendix B for our results.

Table 4.4 Minimum, maximum and mean distance error of our results

Landmark	Horizontal distance (mm.)			Vertical distance (mm.)			Euclidean distance (mm.)		
	Min	Max	Mean	Min	Max	Mean	Min	Max	Mean
Ear rod	0	0.59	0.15	0	0.34	0.15	0.08	0.62	0.24
Porion	-8.22	7.03	0.34	-14.9	10.5	-2.54	0.49	16.14	6.09
Sella	-11.1	15.7	0.87	-1.44	17.4	2.72	0.25	21.17	4.52
Nasion	0.85	2.88	0.26	-3.39	8.39	0.45	0.24	8.59	1.76
Orbitale	-5.93	10.33	0.50	-2.63	6.69	0.99	0.57	10.93	3.86
ANS	-3.05	6.01	0.48	-2.96	3.81	0.16	0.35	6.50	1.95
Subspinale	-23.3	6.01	0.41	-8.47	3.73	-0.08	0.19	24.78	3.15
Is	-1.44	17.28	0.74	-8.13	1.69	0.69	0.08	19.10	1.55
Ii	-1.27	8.47	0.80	-0.68	6.10	1.39	0.46	8.47	2.34
Supramentale	-1.44	7.62	0.55	-3.13	7.62	0.87	0.49	10.78	2.21
Pogonion	-1.44	7.20	0.40	-3.39	8.47	0.40	0.08	10.85	2.19
Menton	0	12.96	1.75	-1.19	0	0.49	0.08	12.98	1..98
Gonion	-9.32	2.46	-3.57	-8.05	6.61	1.53	0.84	10.45	5.51

* calculated from 30 images

After analyzing the results, our result errors are from 3 causes. First cause is noise. Since landmark mostly locates on edge, noise is the most effect of edge detection. Even some landmarks are not located on edge such as Porion and Sella, noise is still the cause of missed detection. Second cause is the region of interest (ROI). Some ROIs do not cover the landmark. Thus, it is a big error (see Figure 4.3). The last cause is the shadow especially for Gonion (see Figure 4.4).

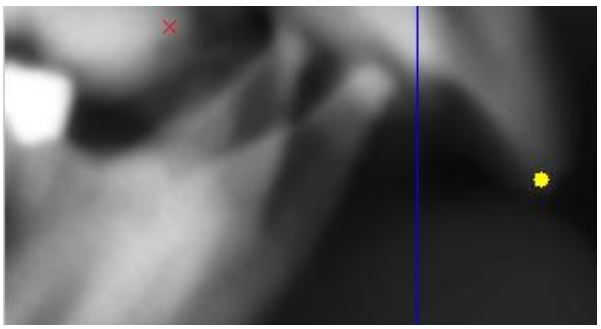

Figure 4.3 Incisor superior detection (red-cross mark means our detected location while yellow circle means the first time detected by orthodontist. Blue line means ends of ROI)

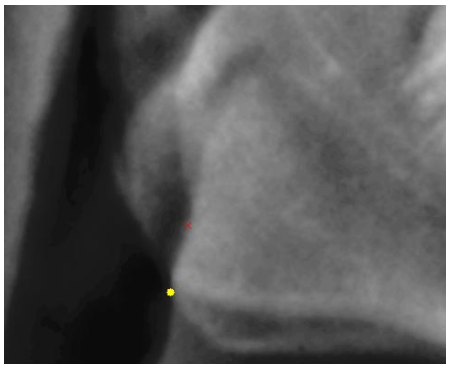

Figure 4.4 Go detection (red cross means our detected location while yellow circle means the first time detected by orthodontist)

Chapter V

Discussions and Conclusions

For conclusion, this work proposed a methodology for automatic Cephalometric landmark detection by creating general rough models for the upper and the lower part of head's structure in order to detect ROI for each landmark, and then identifying landmark location individually using anatomical knowledge and image processing.

Main problem in this work is noise. Since images are scanned with high resolution, there is also much noise. In this work, noise is reduced by Gaussian filtering with approximate SD calculated from image's background. However, most landmarks locate on edge and edge detection is sensitive to noise. It should be another algorithm for noise removal such as multi-resolution technique.

About local enhancement, more anatomical knowledge should be considered with, for example; the knowledge about the intensity of tissue or bones or air, and the information about the percentage of those structures in a specific part of human body.

Some errors are causes by the characteristic of cephalogram, which is the projection of non-symmetric organ such as Porion, Gonion and Orbitale. An example of left and right side of mandibular plane is shown in Figure 5.1. Practically, the location is calculated from average of those two points based on an expert decision.

Figure 5.1 Non-symmetric organ causes two lines of mandibular plane

About our general models, there should be another algorithm to recheck or adjust the model before landmark localization. Moreover, we believe that more images in small range of patient's ages will give a better ROI for each landmark, and makes landmark specifying easier.

Finally, we recommend for the next improvement of this work. The prefer system is a semi-automatic detection which gives initial location of desired landmarks, and allows human to move the points manually.

References

[1] สมศักดิ์ เจิ่งประภากร. Cephalometrics. เอกสารคำสอน วิชา Orthodontic II. ภาควิชาทันตกรรมจัดฟัน คณะทันตแพทย์ศาสตร์ จุฬาลงกรณ์มหาวิทยาลัย

[2] Manosudprasit M. Cephalometric Analysis (In Thai). Orthodontic Text Book. ISBN : 9742844577, pp. 215-228

[3] Ross, A. (2004). Procrustes analysis. Course report, Department of Computer Science and Engineering, University of South Carolina.

[4] Elisseeff, A., and Pontil, M. (2003). Leave-one-out error and stability of learning algorithms with applications. NATO SCIENCE SERIES SUB SERIES III COMPUTER AND SYSTEMS SCIENCES, 190, 111-130.

[5] Rafael C. G., and Richard E. W. Introduction. Digital Image Processing (2nd edition), pp.25-28

[6] Histogram specification [online]. Available from : http://www.cyanogen.com/

[7] Nikos D., and Ross M. Histogram specification [online]. 2012. Available from : http://fourier.eng.hmc.edu/e161/lectures

[8] Edge detection [online].Available from: http://robotics.technion.ac.il (Technion-Israel Institute of Technology, Department of Mechanic Engineering)

[9] Rafael C. G., and Richard E. W. Morphological Image Processing, Digital Image Processing (2nd edition), pp.523-532

[10] Siripanth C., and Covavisarach N. Automatic Cephalometric Landmark Detection: A Survey", in Proc. JICTEE'10, pp. 354-359.

[11] Levy-Mandel, A. D., Venetsanopoulos, A. N., and Tsotsos, J. K. (1986). Knowledge-based landmarking of cephalograms. Computers and Biomedical Research, 19(3), pp.282-309.

[12] Parthasarathy, S., Nugent, S. T., Gregson, P. G., and Fay, D. F. (1989). Automatic landmarking of cephalograms. Computers and Biomedical research, 22(3), pp.248-269.

[13] Davis, D. N., and Taylor, C. J. (1991). A blackboard architecture for automating cephalometric analysis. Informatics for Health and Social Care, 16(2), pp.137-149.

[14] Cardillo, J., and Sid-Ahmed, M. A. (1994). An image processing system for locating craniofacial landmarks. Medical Imaging, IEEE Transactions on, 13(2), pp.275-289.

[15] Grau, V., Alcaniz, M., Juan, M. C., Monserrat, C., and Knoll, C. (2001). Automatic localization of cephalometric landmarks. Journal of Biomedical Informatics, 34(3), pp.146-156.

[16] Rudolph, D. J., Coggins, J. M., and Moon, H. (1997). Investigation of filter sets for supervised pixel classification of cephalometric landmarks by spatial spectroscopy. International journal of medical informatics, 47(3), pp.183-191.

[17] Rudolph, D. J., Sinclair, P. M., and Coggins, J. M. (1998). Automatic computerized radiographic identification of cephalometric landmarks. American Journal of Orthodontics and Dentofacial Orthopedics, 113(2), pp.173-179.

[18] Hutton, T. J., Cunningham, S., and Hammond, P. (2000). An evaluation of active shape models for the automatic identification of cephalometric landmarks. The European Journal of Orthodontics, 22(5), pp.499-508.

[19] Yue, W., Yin, D., Li, C., Wang, G., and Xu, T. (2006). Automated 2-D cephalometric analysis on X-ray images by a model-based approach. Biomedical Engineering, IEEE Transactions on, 53(8), pp.1615-1623.

[20] Rueda, S., and Alcaniz, M. (2006). An approach for the automatic cephalometric landmark detection using mathematical morphology and active appearance models. In Medical Image Computing and Computer-Assisted Intervention–MICCAI 2006 (pp. 159-166). Springer Berlin Heidelberg.

[21] Vucinic, P., Trpovski, Ž., & Ščepan, I. (2010). Automatic landmarking of cephalograms using active appearance models. The European Journal of Orthodontics, 32(3), pp.233-241.

[22] Chen, Y. T., Cheng, K. S., and Liu, J. K. (1999). Improving cephalogram analysis through feature subimage extraction. Engineering in Medicine and Biology Magazine, IEEE, 18(1), pp.25-31.

[23] Ciesielski, V., Innes, A., John, S., and Mamutil, J. (2003). Genetic programming for landmark detection in cephalometric radiology images. International Journal of Knowledge based intelligent engineering Systems, 7(3), pp.164-171.

[24] Innes, A., Ciesielski, V., Mamutil, J., and John, S. (2002, June). Landmark detection for cephalometric radiology images using pulse coupled neural networks. In Proc. Int. Conf. on Artificial Intelligence (Vol. 2).

[25] El-Feghi, I., Sid-Ahmed, M. A., and Ahmadi, M. (2003). Automatic Identification and Localization of Craniofacial Landmarks Using Multi Layer Neural Network. In Medical Image Computing and Computer-Assisted Intervention-MICCAI 2003 (pp. 643-654). Springer Berlin Heidelberg.

[26] El-Feghi, I., Sid-Ahmed, M. A., and Ahmadi, M. (2004). Automatic localization of craniofacial landmarks for assisted cephalometry. Pattern Recognition, 37(3), pp.609-621.

[27] El-Feghi, I., Sid-Ahmed, M. A., and Ahmadi, M. (2006). Automatic localization of craniofacial landmarks using multi-layer perceptron as a function approximator. Pattern recognition letters, 27(6), pp.544-550.

[28] El-Feghi, I., Alginahi, Y., Sid-Ahmed, M. A., & Ahmadi, M. (2004, May). Craniofacial landmarks extraction by partial least squares regression. In Circuits and Systems, 2004. ISCAS'04. Proceedings of the 2004 International Symposium on (Vol. 4, pp. IV-45). IEEE.

[29] Chakrabartty, S., Yagi, M., Shibata, T., and Cauwenberghs, G. (2003, July). Robust cephalometric landmark identification using support vector machines. In Multimedia and Expo, 2003. ICME'03. Proceedings. 2003 International Conference on (Vol. 3, pp. III-429). IEEE.

[30] Mohseni, H., and Kasaei, S. (2007, December). Automatic localization of cephalometric landmarks. In Signal Processing and Information Technology, 2007 IEEE International Symposium on (pp. 396-401). IEEE.

[31] Kafieh, R., Mehri, A., and Sadri, S. (2007, December). Automatic landmark detection in cephalometry using a modified active shape model with sub image matching. In Machine Vision, 2007. ICMV 2007. International Conference on (pp. 73-78). IEEE.

[32] Houston, W. J. B. (1983). The analysis of errors in orthodontic measurements. American journal of orthodontics, 83(5), pp.382-390.

[33] Siripanth C., and Covavisarach N. Automatic Cephalometric Landmark Detection using Procrustes Analysis. In Proc. ICIIP'13, pp. 258-263.

Appendices

Appendix A

Direction used in Appendices

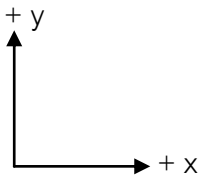

Intra-observer error

Table: Intra-observer error distance of *Ear rod*

Image No.	Δx (mm.)	Δy (mm.)	Euclidean (mm.)
1	-0.17	0.00	0.17
2	0.00	0.25	0.25
3	0.00	0.17	0.17
4	0.25	0.08	0.27
5	0.00	-0.17	0.17
6	0.17	0.00	0.17
7	-0.08	0.00	0.08
8	0.08	0.00	0.08
9	-0.08	0.00	0.08
10	0.17	0.17	0.24
Mean	**0.03**	**0.05**	**0.17**
SD	**0.13**	**0.12**	**0.07**
Min of range	**-0.17**	**-0.17**	**0.08**
Max of range	**0.25**	**0.25**	**0.27**

Table: Intra-observer error distance of *Porion*

Image No.	Δx (mm.)	Δy (mm.)	Euclidean (mm.)
1	1.36	0.34	1.40
2	0.08	0.68	0.68
3	-0.34	-0.68	0.76
4	0.00	1.44	1.44
5	-0.34	-0.08	0.35
6	0.17	2.29	2.29
7	0.25	-0.51	0.57
8	0.25	0.08	0.27
9	-0.17	1.27	1.28
10	-0.08	-0.51	0.52
Mean	**0.12**	**0.43**	**0.96**
SD	**0.49**	**0.98**	**0.63**
Min of range	**-0.34**	**-0.68**	**0.27**
Max of range	**1.36**	**2.29**	**2.29**

Table: Intra-observer error distance of *Sella*

Image No.	Δx (mm.)	Δy (mm.)	Euclidean (mm.)
1	0.08	0.34	0.35
2	0.00	0.25	0.25
3	-0.51	-0.68	0.85
4	0.25	0.08	0.27
5	0.00	0.34	0.34
6	0.08	-0.17	0.19
7	0.00	0.08	0.08
8	-0.08	0.17	0.19
9	0.08	-0.08	0.12
10	-0.08	-0.08	0.12
Mean	**-0.02**	**0.03**	**0.28**
SD	**0.20**	**0.30**	**0.22**
Min of range	**-0.51**	**-0.68**	**0.08**
Max of range	**0.25**	**0.34**	**0.85**

Table: Intra-observer error distance of *Nasion*

Image No.	Δx (mm.)	Δy (mm.)	Euclidean (mm.)
1	-0.08	-0.08	0.12
2	-0.42	0.17	0.46
3	0.42	0.08	0.43
4	0.34	0.00	0.34
5	-0.25	-0.08	0.27
6	-0.59	-0.42	0.73
7	0.08	0.17	0.19
8	-0.08	1.69	1.70
9	0.51	-0.08	0.52
10	-0.17	-0.08	0.19
Mean	-0.02	0.14	0.5
SD	0.36	0.57	0.46
Min of range	-0.59	-0.42	0.12
Max of range	0.51	1.69	1.70

Table: Intra-observer error distance of *Orbitale*

Image No.	Δx (mm.)	Δy (mm.)	Euclidean (mm.)
1	-0.34	0.00	0.34
2	0.08	0.00	0.08
3	0.00	-0.25	0.25
4	2.20	0.17	2.21
5	0.34	-0.34	0.48
6	-2.37	-0.85	2.52
7	0.59	-0.08	0.60
8	-0.25	0.17	0.31
9	0.34	-0.17	0.38
10	-0.76	-0.08	0.77
Mean	-0.02	-0.14	0.79
SD	1.14	0.30	0.85
Min of range	-2.37	-0.85	0.08
Max of range	2.20	0.17	2.52

Table: Intra-observer error distance of *ANS*

Image No.	Δx (mm.)	Δy (mm.)	Euclidean (mm.)
1	0.34	-1.44	1.48
2	-1.78	0.17	1.79
3	0.76	-0.34	0.83
4	1.10	0.08	1.10
5	-0.17	0.34	0.38
6	-0.34	0.00	0.34
7	-0.08	0.08	0.12
8	-1.10	0.42	1.18
9	0.25	0.25	0.36
10	0.00	0.17	0.17
Mean	**-0.10**	**-0.03**	**0.78**
SD	**0.84**	**0.54**	**0.59**
Min of range	**-1.78**	**-1.44**	**0.12**
Max of range	**1.10**	**0.42**	**1.79**

Table: Intra-observer error distance of *Subspinale*

Image No.	Δx (mm.)	Δy (mm.)	Euclidean (mm.)
1	-0.76	0.34	0.83
2	-1.10	0.51	1.21
3	0.34	-0.34	0.48
4	0.42	0.51	0.66
5	0.00	-0.42	0.42
6	0.59	-0.17	0.62
7	-0.76	0.68	1.02
8	-0.34	0.76	0.83
9	0.00	0.93	0.93
10	-0.08	-0.34	0.35
Mean	**-0.17**	**0.25**	**0.74**
SD	**0.56**	**0.51**	**0.28**
Min of range	**-1.10**	**-0.42**	**0.35**
Max of range	**0.59**	**0.93**	**1.21**

Table: Intra-observer error distance of *Incisor superior*

Image No.	Δx (mm.)	Δy (mm.)	Euclidean (mm.)
1	-0.08	0.59	0.60
2	0.25	0.17	0.31
3	-0.42	-0.34	0.54
4	0.08	0.00	0.08
5	-0.34	-0.25	0.42
6	0.17	0.42	0.46
7	0.08	-0.17	0.19
8	-0.17	0.85	0.86
9	0.17	-0.34	0.38
10	-0.25	0.51	0.57
Mean	**-0.05**	**0.14**	**0.44**
SD	**0.23**	**0.43**	**0.22**
Min of range	**-0.42**	**-0.34**	**0.08**
Max of range	**0.25**	**0.85**	**0.86**

Table: Intra-observer error distance of *Incisor inferior*

Image No.	Δx (mm.)	Δy (mm.)	Euclidean (mm.)
1	0.17	0.17	0.24
2	0.00	-0.17	0.17
3	-0.25	0.68	0.72
4	0.25	0.17	0.31
5	-0.17	-0.17	0.24
6	0.17	0.00	0.17
7	0.85	0.34	0.91
8	-0.17	-0.08	0.19
9	0.34	-0.08	0.35
10	-0.25	-0.08	0.27
Mean	**0.09**	**0.08**	**0.36**
SD	**0.34**	**0.27**	**0.25**
Min of range	**-0.25**	**-0.17**	**0.17**
Max of range	**0.85**	**0.68**	**0.91**

Table: Intra-observer error distance of *Supramentale*

Image No.	Δx (mm.)	Δy (mm.)	Euclidean (mm.)
1	-0.08	0.00	0.08
2	-0.85	-1.95	2.12
3	0.08	-0.68	0.68
4	0.93	1.61	1.86
5	-0.08	-0.59	0.60
6	0.08	0.51	0.52
7	-0.08	0.25	0.27
8	-0.25	1.10	1.13
9	0.25	0.08	0.27
10	0.00	0.59	0.59
Mean	**0.00**	**0.09**	**0.81**
SD	**0.44**	**1.00**	**0.69**
Min of range	**-0.85**	**-1.95**	**0.08**
Max of range	**0.93**	**1.61**	**2.12**

Table: Intra-observer error distance of *Pogonion*

Image No.	Δx (mm.)	Δy (mm.)	Euclidean (mm.)
1	0.76	1.78	1.94
2	0.34	0.76	0.83
3	0.17	0.51	0.54
4	0.08	0.42	0.43
5	0.00	0.00	0.00
6	0.00	0.51	0.51
7	-0.42	-1.36	1.42
8	-0.08	0.34	0.35
9	-0.08	-0.51	0.52
10	0.08	0.25	0.27
Mean	**0.09**	**0.27**	**0.68**
SD	**0.31**	**0.82**	**0.58**
Min of range	**-0.42**	**-1.36**	**0.00**
Max of range	**0.76**	**1.78**	**1.94**

Table: Intra-observer error distance of *Menton*

Image No.	Δx (mm.)	Δy (mm.)	Euclidean (mm.)
1	-0.17	-0.25	0.31
2	-0.34	-0.08	0.35
3	0.00	0.34	0.34
4	0.76	0.00	0.76
5	-0.34	0.00	0.34
6	0.42	-0.08	0.43
7	0.25	0.25	0.36
8	0.08	0.17	0.19
9	0.25	0.00	0.25
10	-1.02	0.17	1.03
Mean	**-0.01**	**0.05**	**0.44**
SD	**0.49**	**0.18**	**0.26**
Min of range	**-1.02**	**-0.25**	**0.19**
Max of range	**0.76**	**0.34**	**1.03**

Table: Intra-observer error distance of *Gonion*

Image No.	Δx (mm.)	Δy (mm.)	Euclidean (mm.)
1	1.78	-0.25	1.8
2	-0.34	0.42	0.54
3	0.42	-0.68	0.8
4	-0.17	1.86	1.87
5	0.68	-0.93	1.15
6	0.08	0.25	0.27
7	-1.36	1.95	2.37
8	0.68	-0.34	0.76
9	-0.17	0.76	0.78
10	-0.51	1.02	1.14
Mean	0.11	0.41	1.15
SD	0.85	1	0.67
Min of range	-1.36	-0.93	0.27
Max of range	1.78	1.95	2.37

Appendix B

Our results

Table: Error distance of Ear rod

Image No.	Δx (mm.)	Δy (mm.)	Euclidean (mm.)	Image No.	Δx (mm.)	Δy (mm.)	Euclidean (mm.)
1	0.00	-0.34	0.34	18	0.00	-0.08	0.08
2	0.00	0.08	0.08	19	-0.17	0.08	0.19
3	0.17	0.17	0.24	20	0.25	-0.17	0.31
4	0.34	-0.08	0.35	21	0.17	-0.08	0.19
5	0.08	-0.25	0.27	22	0.08	0.00	0.08
6	0.17	-0.08	0.19	23	0.17	-0.08	0.19
7	-0.08	-0.25	0.27	24	0.34	0.00	0.34
8	0.08	-0.08	0.12	25	0.34	-0.34	0.48
9	0.00	-0.25	0.25	26	0.25	-0.17	0.31
10	0.17	-0.17	0.24	27	0.08	-0.34	0.35
11	0.17	0.08	0.19	28	-0.08	-0.25	0.27
12	0.08	-0.25	0.27	29	0.17	0.00	0.17
13	0.59	-0.17	0.62	30	0.25	-0.17	0.31
14	0.08	-0.08	0.12	Mean	0.13	-0.12	0.25
15	0.08	-0.17	0.19	SD	0.15	0.13	0.12
16	0.17	0.00	0.17	Min of range	-0.17	-0.34	0.08
17	0.00	-0.17	0.17	Max of range	0.59	0.17	0.62

Table: Error distance of Porion

Image No.	Δx (mm.)	Δy (mm.)	Euclidean (mm.)	Image No.	Δx (mm.)	Δy (mm.)	Euclidean (mm.)
1	0.85	-3.3	3.41	18	-6.18	-14.91	16.14
2	-2.37	-7.62	7.98	19	-1.27	10.5	10.58
3	-3.56	-9.23	9.89	20	1.19	-3.3	3.51
4	1.44	5.17	5.36	21	-0.25	0.42	0.49
5	-6.86	-10.93	12.9	22	0.34	5.76	5.77
6	3.22	2.54	4.1	23	3.64	4.74	5.98
7	1.36	1.86	2.3	24	6.95	-3.13	7.62
8	-3.56	-1.78	3.98	25	-3.39	-7.71	8.42
9	0.51	-3.05	3.09	26	-2.29	-5.76	6.2
10	2.63	-3.64	4.49	27	-0.68	-2.46	2.55
11	-0.51	-4.57	4.6	28	-7.03	-1.86	7.27
12	-3.39	-3.9	5.16	29	3.22	-8.3	8.9
13	5.17	4.57	6.9	30	-2.46	-2.8	3.72
14	-3.98	-0.68	4.04	Mean	-0.33	-2.47	6.12
15	8.22	-2.71	8.65	SD	3.78	5.41	3.35
16	1.61	-6.44	6.64	Min of range	-7.03	-14.91	0.49
17	-2.46	-1.44	2.85	Max of range	8.22	10.5	16.14

Table: Error distance of Sella

Image No.	Δx (mm.)	Δy (mm.)	Euclidean (mm.)	Image No.	Δx (mm.)	Δy (mm.)	Euclidean (mm.)
1	4.66	-6.69	8.15	18	-0.85	0.08	0.85
2	-4.49	-9.66	10.65	19	0.42	1.27	1.34
3	-4.57	-17.7	18.28	20	0.00	-0.42	0.42
4	-1.27	0.00	1.27	21	0.51	0.25	0.57
5	0.25	0.17	0.31	22	0.00	0.85	0.85
6	1.02	0.00	1.02	23	0.25	-0.17	0.31
7	-0.08	1.10	1.10	24	-0.59	-1.27	1.40
8	11.01	-0.51	11.02	25	1.86	-13.89	14.02
9	-1.27	1.44	1.92	26	-2.96	-12.45	12.80
10	0.00	0.51	0.51	27	-0.34	-1.10	1.15
11	-0.25	0.17	0.31	28	-0.25	0.76	0.80
12	-15.75	-14.14	21.17	29	0.08	-0.25	0.27
13	0.68	1.27	1.44	30	-1.61	0.42	1.66
14	1.78	-1.44	2.29	Mean	-0.88	-2.71	4.53
15	-1.36	1.02	1.69	SD	4.52	5.67	6.31
16	-12.54	-11.69	17.14	Min of range	-15.75	-17.7	0.27
17	-0.76	0.76	1.08	Max of range	11.01	1.44	21.17

Table: Error distance of Nasion

Image No.	Δx (mm.)	Δy (mm.)	Euclidean (mm.)	Image No.	Δx (mm.)	Δy (mm.)	Euclidean (mm.)
1	0.76	1.61	1.78	18	0.59	-0.17	0.62
2	0.34	0.76	0.83	19	-2.12	-2.54	3.31
3	0.59	0.76	0.97	20	-0.08	0.85	0.85
4	0.42	0.42	0.60	21	-0.25	0.25	0.36
5	-0.76	-0.42	0.87	22	0.17	0.17	0.24
6	-0.17	0.34	0.38	23	0.00	0.34	0.34
7	-1.19	-5.84	5.96	24	-0.42	-0.08	0.43
8	0.34	4.24	4.25	25	-0.34	0.25	0.42
9	0.76	2.12	2.25	26	0.08	2.2	2.2
10	-0.59	0.17	0.62	27	-2.88	-4.83	5.62
11	-1.86	-8.39	8.59	28	-0.76	-2.54	2.65
12	-1.19	-4.91	5.05	29	-0.51	-0.59	0.78
13	0.00	0.25	0.25	30	0.00	0.34	0.34
14	0.17	-0.17	0.24	Mean	-0.27	-0.41	1.79
15	0.17	0.93	0.95	SD	0.86	2.60	2.10
16	0.17	0.85	0.86	Min of range	-2.88	-8.39	0.24
17	0.34	1.19	1.23	Max of range	0.76	4.24	8.59

Table: Error distance of Orbitale

Image No.	Δx (mm.)	Δy (mm.)	Euclidean (mm.)	Image No.	Δx (mm.)	Δy (mm.)	Euclidean (mm.)
1	5.76	2.63	6.33	18	-5.84	-1.69	6.08
2	1.44	-1.69	2.22	19	-10.33	-3.56	10.93
3	5.34	-5.17	7.43	20	1.27	-0.34	1.31
4	-0.34	-1.02	1.07	21	1.95	0.17	1.96
5	-5.84	0.42	5.86	22	-4.74	-0.51	4.77
6	3.13	0.08	3.14	23	-0.34	-0.93	0.99
7	0.93	-0.25	0.97	24	-4.83	0.00	4.83
8	0.68	-0.25	0.72	25	-1.44	-0.25	1.46
9	2.03	-0.25	2.05	26	-0.51	-0.25	0.57
10	3.98	-0.59	4.02	27	1.19	-5.17	5.30
11	5.42	-6.69	8.61	28	-3.9	0.08	3.90
12	-2.46	-2.20	3.30	29	2.12	-0.76	2.25
13	1.44	-1.19	1.87	30	-9.40	2.63	9.76
14	-2.37	-0.85	2.52	Mean	-0.51	-1.01	3.78
15	0.68	-0.93	1.15	SD	4.14	1.98	2.77
16	-3.90	-1.61	4.22	Min of range	-10.33	-6.69	0.57
17	3.73	-0.08	3.73	Max of range	5.76	2.63	10.93

Table: Error distance of ANS

Image No.	Δx (mm.)	Δy (mm.)	Euclidean (mm.)	Image No.	Δx (mm.)	Δy (mm.)	Euclidean (mm.)
1	0.08	0.17	0.19	18	1.02	0.25	1.05
2	1.19	0.00	1.19	19	-3.73	-0.85	3.82
3	0.00	-0.34	0.34	20	3.05	2.96	4.25
4	2.63	0.42	2.66	21	0.08	0.34	0.35
5	-1.95	-0.25	1.96	22	0.76	0.17	0.78
6	0.68	0.34	0.76	23	-1.95	0.08	1.95
7	-0.85	-0.85	1.20	24	1.02	0.59	1.18
8	-0.68	0.59	0.90	25	-1.27	-0.76	1.48
9	-1.95	-0.51	2.01	26	-0.85	-0.25	0.88
10	-2.37	0.17	2.38	27	-5.25	0.17	5.25
11	-0.51	0.00	0.51	28	-1.27	0.25	1.30
12	-6.01	-2.46	6.50	29	2.46	-1.61	2.94
13	0.85	0.00	0.85	30	-2.46	0.08	2.46
14	-0.76	-0.51	0.92	Mean	-0.51	-0.16	1.92
15	3.05	1.19	3.27	SD	2.17	1.13	1.56
16	0.34	-3.81	3.83	Min of range	-6.01	-3.81	0.19
17	-0.51	-0.25	0.57	Max of range	3.05	2.96	6.50

Table: Error distance of Subspinale

Image No.	Δx (mm.)	Δy (mm.)	Euclidean (mm.)	Image No.	Δx (mm.)	Δy (mm.)	Euclidean (mm.)
1	-1.27	-1.19	1.74	18	0.00	-2.12	2.12
2	-0.34	-2.63	2.65	19	-2.54	-0.17	2.55
3	0.42	-2.20	2.24	20	3.64	-3.73	5.21
4	-1.27	-2.29	2.62	21	-1.52	-1.44	2.10
5	-1.95	-1.27	2.33	22	-2.37	-0.85	2.52
6	-0.08	0.85	0.85	23	-4.07	0.08	4.07
7	-0.85	1.52	1.74	24	-1.19	-0.25	1.21
8	-1.27	1.95	2.33	25	-2.80	-1.95	3.41
9	-2.29	5.51	5.96	26	0.17	0.34	0.38
10	23.21	8.30	24.65	27	-4.07	4.07	5.75
11	-2.80	2.37	3.67	28	-0.17	-0.08	0.19
12	-6.01	0.34	6.02	29	-1.27	-1.19	1.74
13	-1.52	0.17	1.53	30	0.17	1.52	1.53
14	-0.34	-0.34	0.48	Mean	-0.45	0.13	3.18
15	0.59	-1.52	1.64	SD	4.80	2.49	4.36
16	-1.61	0.59	1.72	Min of range	-6.01	-3.73	0.19
17	-0.08	-0.51	0.52	Max of range	23.21	8.30	24.65

Table: Error distance of Incisor superior

Image No.	Δx (mm.)	Δy (mm.)	Euclidean (mm.)	Image No.	Δx (mm.)	Δy (mm.)	Euclidean (mm.)
1	-17.36	8.47	19.32	18	0.00	0.93	0.93
2	-1.27	1.02	1.63	19	-1.36	-0.08	1.36
3	-1.95	3.39	3.91	20	-0.08	0.68	0.68
4	0.25	0.00	0.25	21	-0.17	0.08	0.19
5	0.25	-0.17	0.31	22	0.34	0.68	0.76
6	-1.36	-0.34	1.40	23	0.25	0.51	0.57
7	1.44	-0.42	1.50	24	0.42	0.34	0.54
8	-0.17	-0.42	0.46	25	0.17	0.08	0.19
9	-1.19	2.63	2.88	26	-0.93	2.29	2.47
10	-0.42	0.85	0.95	27	0.00	0.51	0.51
11	0.25	0.08	0.27	28	0.42	0.08	0.43
12	-0.08	0.85	0.85	29	-0.08	-0.17	0.19
13	-0.17	0.85	0.86	30	0.34	0.25	0.42
14	-0.08	0.00	0.08	Mean	-0.75	0.72	1.53
15	-0.17	-1.69	1.70	SD	3.21	1.75	3.48
16	0.08	0.00	0.08	Min of range	-17.36	-1.69	0.08
17	0.00	0.17	0.17	Max of range	1.44	8.47	19.32

Table: Error distance of Incisor inferior

Image No.	Δx (mm.)	Δy (mm.)	Euclidean (mm.)	Image No.	Δx (mm.)	Δy (mm.)	Euclidean (mm.)
1	-6.95	-3.73	7.88	18	-8.39	-0.85	8.43
2	-0.42	-1.44	1.50	19	-0.17	-3.81	3.82
3	-3.73	-2.03	4.25	20	-0.51	-0.25	0.57
4	-1.78	-2.29	2.90	21	0.34	-1.44	1.48
5	0.17	-1.44	1.45	22	0.76	-0.85	1.14
6	0.42	-0.76	0.87	23	0.51	-0.93	1.06
7	0.85	-1.10	1.39	24	0.68	-1.27	1.44
8	-8.55	0.08	8.56	25	0.85	-1.44	1.67
9	0.34	-0.76	0.83	26	0.85	-1.69	1.89
10	0.68	-0.51	0.85	27	0.25	0.68	0.72
11	0.42	-2.03	2.08	28	0.42	-0.17	0.46
12	1.27	-6.10	6.23	29	-0.34	-0.76	0.83
13	0.42	-0.17	0.46	30	0.08	-0.59	0.60
14	0.68	-1.10	1.29	Mean	-0.79	-1.37	2.34
15	-1.61	-1.10	1.95	SD	2.64	1.32	2.37
16	-1.27	-2.20	2.54	Min of range	-8.55	-6.1	0.46
17	0.00	-1.10	1.10	Max of range	1.27	0.68	8.56

Table: Error distance of Supramentale

Image No.	Δx (mm.)	Δy (mm.)	Euclidean (mm.)	Image No.	Δx (mm.)	Δy (mm.)	Euclidean (mm.)
1	-0.68	-0.76	1.02	18	0.34	-1.61	1.64
2	-1.19	-1.36	1.80	19	-6.10	-2.37	6.54
3	-0.93	-1.95	2.16	20	0.17	-0.51	0.54
4	1.44	2.29	2.70	21	0.08	-1.19	1.19
5	0.51	2.46	2.51	22	-0.25	-1.02	1.05
6	0.85	-1.44	1.67	23	-0.34	-2.46	2.48
7	0.51	2.71	2.76	24	-0.68	-3.81	3.87
8	-0.42	0.25	0.49	25	-0.68	-0.85	1.08
9	0.51	1.02	1.14	26	-1.95	-3.73	4.21
10	-0.08	-0.93	0.94	27	-0.17	-2.03	2.04
11	0.34	-1.61	1.64	28	0.51	0.59	0.78
12	-0.25	-0.51	0.57	29	-1.27	-0.17	1.28
13	0.68	0.85	1.08	30	-0.08	-2.12	2.12
14	-7.62	-7.62	10.78	Mean	-0.56	-0.88	2.20
15	-0.08	-1.78	1.78	SD	1.87	2.16	2.07
16	0.93	3.13	3.27	Min of range	-7.62	-7.62	0.49
17	-0.85	0.17	0.86	Max of range	1.44	3.13	10.78

Table: Error distance of Pogonion

Image No.	Δx (mm.)	Δy (mm.)	Euclidean (mm.)	Image No.	Δx (mm.)	Δy (mm.)	Euclidean (mm.)
1	0.59	1.52	1.64	18	-0.93	-0.42	1.02
2	0.17	0.51	0.54	19	-7.20	-5.51	9.06
3	0.51	1.10	1.21	20	0.08	0.93	0.94
4	0.34	0.68	0.76	21	0.08	-0.34	0.35
5	-0.17	0.59	0.62	22	0.93	1.61	1.86
6	0.00	2.29	2.29	23	1.02	1.86	2.12
7	-0.34	0.76	0.83	24	1.02	2.37	2.58
8	-0.76	1.02	1.27	25	-0.25	-1.02	1.05
9	-0.17	0.85	0.86	26	0.59	3.39	3.44
10	-0.51	0.25	0.57	27	0.68	2.96	3.04
11	-0.76	-3.3	3.39	28	-0.08	2.54	2.54
12	-1.10	2.63	2.85	29	1.10	2.88	3.08
13	-0.08	1.10	1.10	30	1.44	2.54	2.92
14	-6.78	-8.47	10.85	Mean	-0.39	0.42	2.21
15	-0.17	-1.61	1.62	SD	1.91	2.55	2.32
16	0.08	0.34	0.35	Min of range	-7.20	-8.47	0.35
17	-1.02	-1.36	1.69	Max of range	1.44	3.39	10.85

Table: Error distance of Menton

Image No.	Δx (mm.)	Δy (mm.)	Euclidean (mm.)	Image No.	Δx (mm.)	Δy (mm.)	Euclidean (mm.)
1	-0.34	0.76	0.83	18	-3.56	-0.25	3.57
2	-0.42	0.42	0.60	19	-12.96	-0.68	12.98
3	-1.52	0.42	1.58	20	-0.17	0.93	0.95
4	0.08	0.93	0.94	21	-0.93	0.59	1.10
5	-0.85	-0.51	0.99	22	0.51	0.93	1.06
6	-1.78	0.76	1.94	23	1.36	0.25	1.38
7	0.76	0.34	0.83	24	1.61	0.34	1.64
8	-0.17	0.34	0.38	25	1.95	-0.08	1.95
9	0.34	0.17	0.38	26	2.2	0.51	2.26
10	-0.85	1.27	1.53	27	1.78	0.76	1.94
11	0.00	0.08	0.08	28	2.20	0.00	2.2
12	0.08	0.34	0.35	29	1.95	0.00	1.95
13	-0.85	0.76	1.14	30	0.25	0.93	0.97
14	-11.69	-0.42	11.7	Mean	-0.75	0.37	2.00
15	-1.78	0.59	1.87	SD	3.42	0.48	2.91
16	0.08	0.76	0.77	Min of range	-12.96	-0.68	0.08
17	0.25	-0.08	0.27	Max of range	2.2	1.27	12.98

Table: Error distance of Gonion

Image No.	Δx (mm.)	Δy (mm.)	Euclidean (mm.)	Image No.	Δx (mm.)	Δy (mm.)	Euclidean (mm.)
1	5.51	-2.54	6.06	18	-0.85	4.49	4.57
2	0.68	0.68	0.96	19	-2.46	8.05	8.41
3	7.62	0.85	7.67	20	5.25	-4.24	6.75
4	-1.02	4.74	4.85	21	7.54	-6.61	10.02
5	1.61	6.18	6.39	22	3.22	-1.78	3.68
6	2.80	-4.24	5.07	23	1.52	-1.61	2.22
7	1.27	1.69	2.12	24	3.30	-4.91	5.92
8	4.15	-4.57	6.18	25	3.47	-4.74	5.88
9	0.59	-0.59	0.84	26	5.08	-5.08	7.19
10	5.25	-0.42	5.27	27	7.37	-4.32	8.54
11	5.84	-3.05	6.59	28	4.49	-5.67	7.24
12	6.35	2.54	6.84	29	4.57	-6.52	7.97
13	2.54	-2.03	3.25	30	3.05	-0.76	3.14
14	9.32	-4.74	10.45	Mean	3.57	-1.53	5.51
15	6.27	-4.40	7.66	SD	2.84	3.82	2.62
16	0.93	-0.93	1.32	Min of range	-2.46	-6.61	0.84
17	1.78	-1.36	2.24	Max of range	9.32	8.05	10.45

Biography

Miss Chalermkwan Siripanth was born on February 17, 1987 in Bangkok, Thailand. She had graduated Bachelor of Engineering with second class honors in 2009 from Department of Computer Engineering, Faculty of Engineering, Chulalongkorn University, Thailand. Then, she started studying the Degree of Master of Science Program in Biomedical Engineering at Chulalongkorn University, Bangkok, Thailand in 2009. While studying, she published her research with her advisor under the topic "Automatic Cephalometric Landmark Detection: A Survey" in the joint International Conference of Information and Communication Technology, Electronic and Electrical Engineering (JICTEE 2010) held on 21-24 December 2010. This article was also published in conference proceeding of JICTEE-2010 Luang Prabang, Lao PRD. Dec 21 - Dec 24, 2010, page 354-359. She was also a participant in the 8th International Conference on Intelligent Information Processing (ICIIP 2013) with her topic "Cephalometric Landmark Region Detection using Procrustes Analysis". The conference was held on 1-3 April 2013 in Seoul, South Korea.